Tectonophysics 554–557 (2012) 83–104

Contents lists available at SciVerse ScienceDirect

Tectonophysics

journal homepage: www.elsevier.com/locate/tecto

Shear wave velocity structure of the Bushveld Complex, South Africa

Eldridge M. Kgaswane [a,c,*], Andrew A. Nyblade [b], Raymond J. Durrheim [c,e], Jordi Julià [f], Paul H.G.M. Dirks [c,d], Susan J. Webb [c]

[a] Council for Geoscience, 280 Pretoria Road, Private Bag X112, Pretoria 0001, South Africa
[b] Department of Geosciences, Pennsylvania State University, University Park, PA, USA
[c] School of Geosciences, University of the Witwatersrand, Private Bag 3, Johannesburg 2050, South Africa
[d] School of Earth and Environmental Sciences, James Cook University, Townsville Qld 4811, Australia
[e] Council for Scientific and Industrial Research, cnr Rustenburg and Carlow Roads, Johannesburg, South Africa
[f] Departamento de Geofísica & Programa de Pós-Graduação em Geodinâmica e Geofísica, Universidade Federal do Rio Grando do Norte, Natal, Rio Grande do Norte, Brazil

ARTICLE INFO

Article history:
Received 27 September 2011
Received in revised form 4 May 2012
Accepted 3 June 2012
Available online 15 June 2012

Keywords:
Bushveld Complex
Continuous-sheet model
Dipping-sheet model
Joint inversion
Receiver functions
Rayleigh wave group velocities

ABSTRACT

The structure of the crust in the environs of the Bushveld Complex has been investigated by jointly inverting high-frequency teleseismic receiver functions and 2–60 s period Rayleigh wave group velocities for 16 broadband seismic stations located across the Bushveld Complex. Group velocities for 2–15 s periods were obtained from surface wave tomography using local and regional events, while group velocities for 20–60 s periods were taken from a published model. 1-D shear wave velocity models obtained for each station show the presence of thickened crust in the center of the Bushveld Complex and a region at the base of the crust where shear wave velocities exceed 4.0 km/s. The shear wave velocity models also suggest that velocities in some upper crustal layers may be as high as 3.7–3.8 km/s, consistent with the presence of mafic lithologies. These results favor a continuous-sheet model for the Bushveld Complex in which the outcropping mafic layers of the western and eastern limbs are continuous at depth beneath the center of the complex. However, detailed modeling of receiver functions at one station within the center of the complex indicates that the mafic layering may be locally disrupted due to thermal diapirism triggered by the emplacement of the Bushveld Complex or thermal and tectonic reactivation at a later time.

1. Introduction

The Bushveld Complex (BC; ~2.06 Ga) is one of the largest layered mafic igneous intrusions in the world, covering an area of ~66 000 km^2 within the northern Kaapvaal Craton, South Africa (Fig. 1a; e.g., Eglington and Armstrong, 2004; Walraven, 1997; Webb et al., 2004). It hosts the world's largest deposits of platinum group metals, as well as large reserves of chromium, titanium, vanadium, nickel and gold (e.g., Cawthorn et al., 2006). The BC, which intruded into the intracratonic sedimentary sequences of the Transvaal Supergroup (e.g., Cawthorn and Webb, 2001), can be divided into the Rooiberg Group (RG), the Rashoop Granophyre Suite (RGS), the Lebowa Granite Suite (LGS) and the Rustenburg Layered Suite (RLS; e.g., Cawthorn et al., 2006; Hatton and Schweitzer, 1995; South African Committee for Stratigraphy, 1980). Fig. 1 shows the distribution of the different lithologies around the BC. The mafic units of the RLS crop out in five geographically distinct areas, the Eastern Limb, the Western Limb, the Far Western Limb and the two Northern limbs (Fig. 1; e.g., Webb et al., 2004). A sixth limb, the Southeastern or Bethal Limb (Cawthorn and Webb, 2001), is buried under Karoo sediments. The BC is disrupted in several places by alkaline intrusions (Fig. 1).

The deep structure and emplacement history of the BC remain uncertain. The BC was initially described as an internally layered laccolithic (Jorissen, 1904; Mellor, 1906; Molengraaff, 1901) or lopolithic structure (e.g., Du Toit, 1954; Hall, 1932; Molengraaff, 1902), but gravity modeling by Cousins (1959) showed that a Bouguer gravity low associated with the central region of the BC was not consistent with these interpretations. Cousins (1959) suggested that the BC consisted of separate intrusive limbs, with each limb having its own magma feeder system. Cousins (1959) model underwent several refinements, resulting in a model with detached inward dipping bodies (e.g., the "dipping-sheet model"; Biesheuvel, 1970; Du Plessis and Kleywegt, 1987; Meyer and De Beer, 1987; Molyneux and Klinkert, 1978; Van der Merwe, 1976; Walraven and Darracott, 1976). Through additional modeling of gravity data, the "dipping-sheet model" was refined further by Meyer and De Beer (1987), who showed that the limbs could extend to depths of 15 km with no compensation at the Moho (Fig. 2a).

The gravity modeling by Meyer and De Beer (1987) was constrained by deep electrical soundings and resistivity observations, which indicated the presence of a conductive layer beneath the

* Corresponding author at: Council for Geoscience, Private Bag X112, Pretoria 0001, South Africa. Tel.: +27 12 841 1197; fax: +27 866788423.
E-mail address: ekgaswane@geoscience.org.za (E.M. Kgaswane).

0040-1951/$ – see front matter © 2012 Elsevier B.V. All rights reserved.
doi:10.1016/j.tecto.2012.06.003

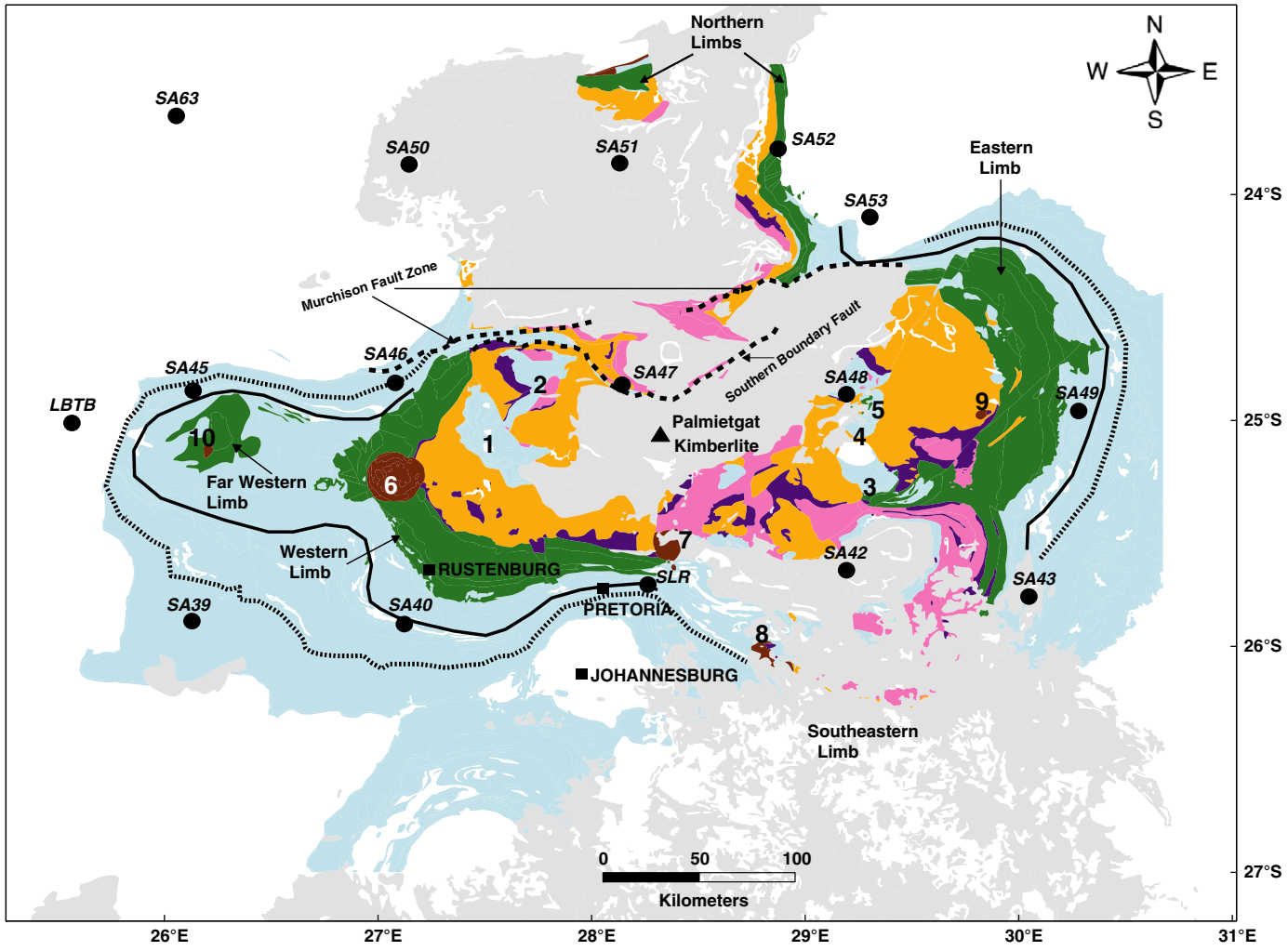
Northern Limbs
Eastern Limb
Southeastern Limb
Western Limb
Far Western Limb
Murchison Fault Zone
Southern Boundary Fault
Palmietgat Kimberlite
RUSTENBURG
PRETORIA
JOHANNESBURG
SLR
SA39
SA40
SA42
SA43
SA45
SA46
SA47
SA48
SA49
SA50
SA51
SA52
SA53
SA63
LBTB
1
2
3
4
5
6
7
8
9
10
N
W
E
S
24°S
25°S
26°S
27°S
26°E
27°E
28°E
29°E
30°E
31°E
0
50
100
Kilometers

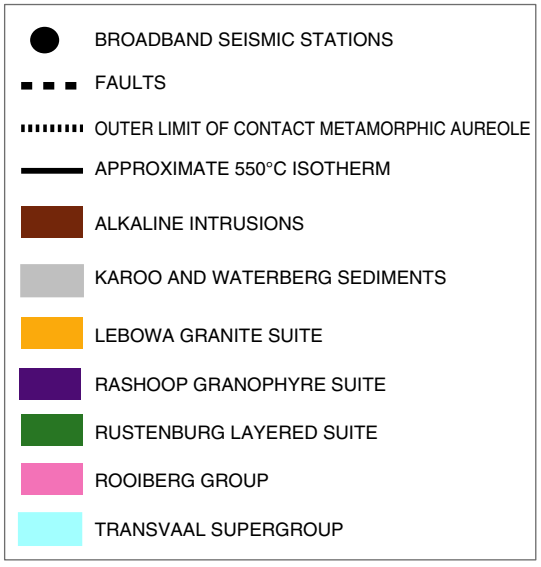
BROADBAND SEISMIC STATIONS
FAULTS
OUTER LIMIT OF CONTACT METAMORPHIC AUREOLE
APPROXIMATE 550°C ISOTHERM
ALKALINE INTRUSIONS
KAROO AND WATERBERG SEDIMENTS
LEBOWA GRANITE SUITE
RASHOOP GRANOPHYRE SUITE
RUSTENBURG LAYERED SUITE
ROOIBERG GROUP
TRANSVAAL SUPERGROUP

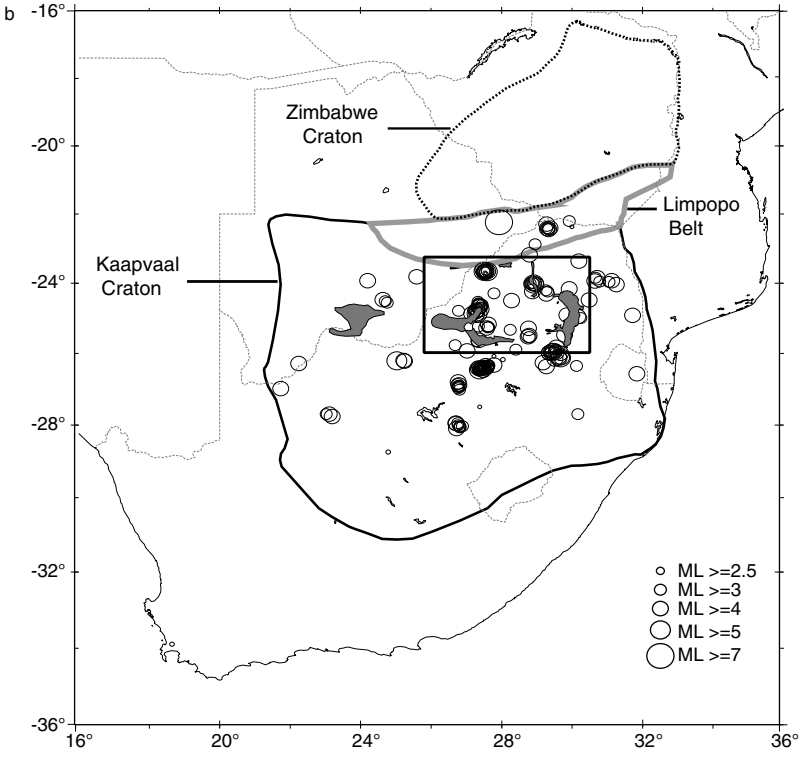
b
Zimbabwe Craton
Kaapvaal Craton
Limpopo Belt
ML >=2.5
ML >=3
ML >=4
ML >=5
ML >=7
-16°
-20°
-24°
-28°
-32°
-36°
16°
20°
24°
28°
32°
36°

granites of the western and eastern limbs of the BC. Meyer and De Beer (1987) attributed this conductive layer to the Silverton shales of the Transvaal Supergroup. An alternative interpretation by Webb et al. (2004) of these resistivity observations based on drilling results of Walraven (1987) indicates that the conductive layer could be related to the rocks of the RLS.

More recent studies, based on geological observations and modeled gravity data, (Cawthorn and Webb, 2001; Cawthorn et al., 1998; Webb et al., 2004) have proposed the existence of continuous mafic layering at depth across the central region of the BC connecting the various limbs (Fig. 2b). In this model, hereinafter called the "continuous-sheet" model, the continuous mafic layering in the upper crust is isostatically compensated for by a depressed Moho, consistent with seismic constraints provided by receiver function studies (Kgaswane et al., 2009; Nair et al., 2006; Nguuri et al., 2001). The seismic velocity model of Nguuri et al. (2001) also shows a high shear wave velocity layer (Vs ~ 4.0 km/s) within the upper 10 km of the crust for one location near the center of the BC. Additional evidence supporting a model with continuous mafic layering under the center of the BC comes from mafic xenoliths found in the Palmietgat kimberlite pipe (Fig. 1; Webb et al., 2010).

The purpose of this paper is to use new seismic velocity models of the BC crust to evaluate the "dipping-sheet" and "continuous-sheet" models. The seismic velocity models are obtained by first measuring short-period Rayleigh wave group velocities using locally and regionally recorded seismic events, and then jointly inverting the group velocity measurements with high-frequency receiver functions. This study differs in two ways from the study by Kgaswane et al. (2009), which used a similar approach. Firstly, to improve constraints on the upper crustal velocity structure, we developed group velocity maps for short-period Rayleigh waves (2–15 s). Secondly, to improve resolution of fine-scale crustal structure, particularly in the upper crust, we used high-frequency ($f \leq 1.25$ Hz) receiver functions in the joint inversions with the group velocities. The study by Kgaswane et al. (2009) investigated the S-wave velocity structure of the crust in southern Africa by jointly inverting high- and low-frequency receiver functions with Rayleigh wave group velocity curves in the period range of 10–175 s. The results of this study provide better resolved shear wave velocity models for locations across the BC and yield new insights into the deep structure of the BC.

2. Data and methods

In this section, we first describe our Rayleigh wave tomography method to obtain group velocity maps for periods between 2 and 15 s. We follow this with a brief description of our methodology for computing receiver functions, and then explain how the two data sets have been jointly inverted.

2.1. Group velocity tomography

A total of 197 mining-related and regional tectonic earthquakes recorded by 45 broadband seismic stations were used for making Rayleigh wave group velocity measurements. The seismic events used have local magnitudes (ML) greater than 2.5 (Fig. 1b). An event list is provided as Supplemental material. Fig. 2c shows the location of the broadband seismic stations with respect to the outcrop pattern of the BC. Forty-three (43) of the stations belong to the Southern African Seismic Experiment (SASE) network (Carlson et al., 1996) and two of the stations belong to the Global Seismic Network (GSN) and South African National Seismograph Network (SANSN). Event catalogs (origin time, hypocenters and local magnitudes) were compiled from the earthquake bulletins published by the Council for Geoscience, by gold mines in the Witwatersrand Basin area and by the Incorporated Research Institutions for Seismology (IRIS). Mining-related earthquakes account for 81% of the total number of earthquakes used for the measurements, the majority of which originated within the gold mining districts of the Witwatersrand Basin.

To measure Rayleigh wave group velocities at each period, a code from Ammon (2001) was used based on multiple filter analysis (e.g., Claerbout, 1992; Dziewonski et al., 1969; Keilis-Borok, 1989; Levshin et al., 1992). The ray coverage is shown in Fig. 3, along with the total number of rays for each period. Ray coverage is greater at shorter periods (2–8 s) compared to longer periods (10–15 s). At each period the ensemble of measurements vary by no more than 0.1–0.2 km/s (see Supplemental material).

The group velocity measurements were inverted using a conjugate gradient algorithm (LSQR) based on the method by Paige and Saunders (1982). The LSQR algorithm solves the following equation:

$$\begin{bmatrix} A \\ \lambda \end{bmatrix} [x] = \begin{bmatrix} b \\ 0 \end{bmatrix} \quad (1)$$

where A represents a matrix of ray distances in each cell, x is a vector of group velocity perturbations or slownesses, b is a vector of group velocity travel-times (distance/group velocity) and λ is a Laplacian smoothing constraint. The choice of an optimal smoothing parameter was made by considering the trade-off between model smoothness and travel-time misfit. Fig. 4 shows the results for 2, 4 and 6 s periods. Trial-and-error inversions were performed using smoothing parameters in the range of 0–200, revealing that a smoothing parameter of 100 provides a good balance between data misfit and model smoothness at all periods. Therefore, a smoothing parameter of 100 was used for the group velocity inversions.

We evaluated the resolution of the group velocity tomography using checkerboard tests with 100 km and 125 km checkers (Fig. 5). The rectangles shown with dashed lines enclose the region with best resolution. The 100×100 km checkers are not as well recovered at any period compared to the 125×125 km checkers, indicating that velocity variations are not well resolved at scales less than ~125 km. In addition, at 12 and 15 s period, only velocity variations within the center of the BC can be resolved for the 125×125 km checkers.

The results of the group velocity tomography are shown in Fig. 6. Across the areas of the BC where velocity variations are best resolved, velocities at all periods vary between 2.8 and 3.2 km/s, but do not show a clear spatial correlation from one period to the next. We found group velocities at 10 and 15 s periods to be 10–30% greater than those reported by Pasyanos and Nyblade (2007) and used by Kgaswane et al. (2009). The ray path coverage reported by Pasyanos and Nyblade (2007) is limited at periods of 10 and 15 s compared to periods ≥ 20 s. Pasyanos and Nyblade (2007) did not report uncertainties at 10 and 15 s and Fig. 4 of Pasyanos and Nyblade (2007) shows uncertainties of less than 0.1 km/s for a period of 20 s. Pasyanos and Nyblade (2007) did not report group velocities for periods less than 10 s.

2.2. Receiver functions

A total of 17 stations, including LBTB and SLR (Fig. 1), fall within the area enclosed by the rectangles shown in Fig. 5. High quality

Fig. 1. a. Map of the Bushveld Complex (BC) showing simplified geology and its six limbs (lobes) — the Eastern, Western, Far Western, Southeastern and the two Northern limbs (map modified from the 1:250 000 geology map of South Africa). Numbers 1, 2, 3, 4 and 5 show the position of some of the domes, and numbers 6, 7, 8, 9 and 10 show the location of alkaline intrusions. The locations of the 16 seismic stations for which Vs models are reported are shown with the prefix "SA" followed by the station number. b. Map of southern Africa showing the locations of earthquakes (open circles) used in this study. The solid black rectangle encloses the study area. Outcrops of the BC are shown as gray polygons. The outlines of the Kaapvaal Craton, Limpopo Belt and the Zimbabwe Craton are shown in solid black, gray and dotted lines, respectively.

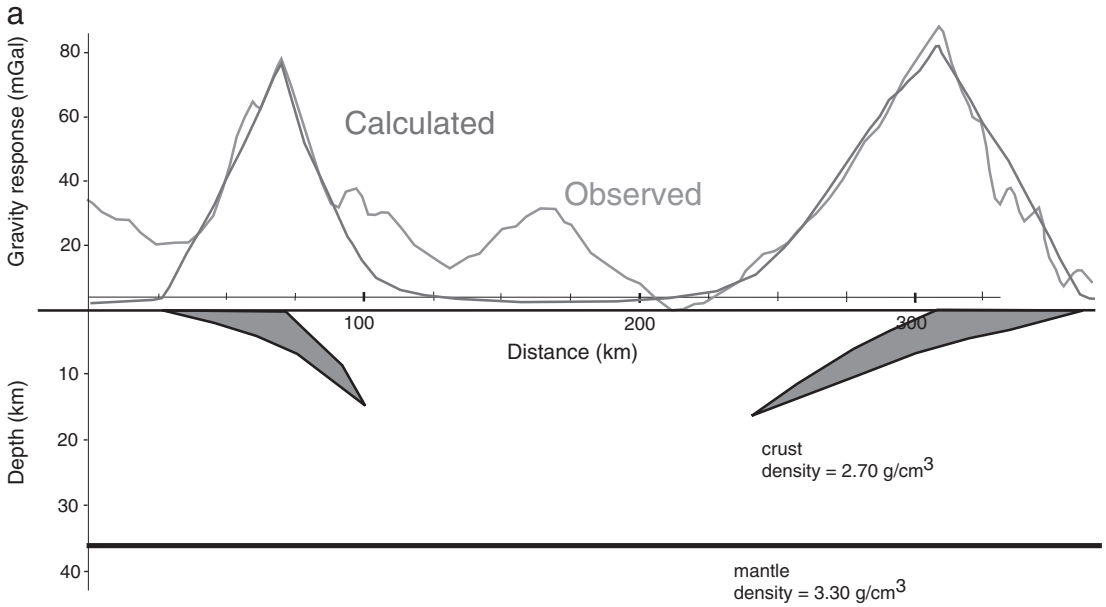
a
Gravity response (mGal)
Calculated
Observed
Distance (km)
Depth (km)
crust
density = 2.70 g/cm3
mantle
density = 3.30 g/cm3

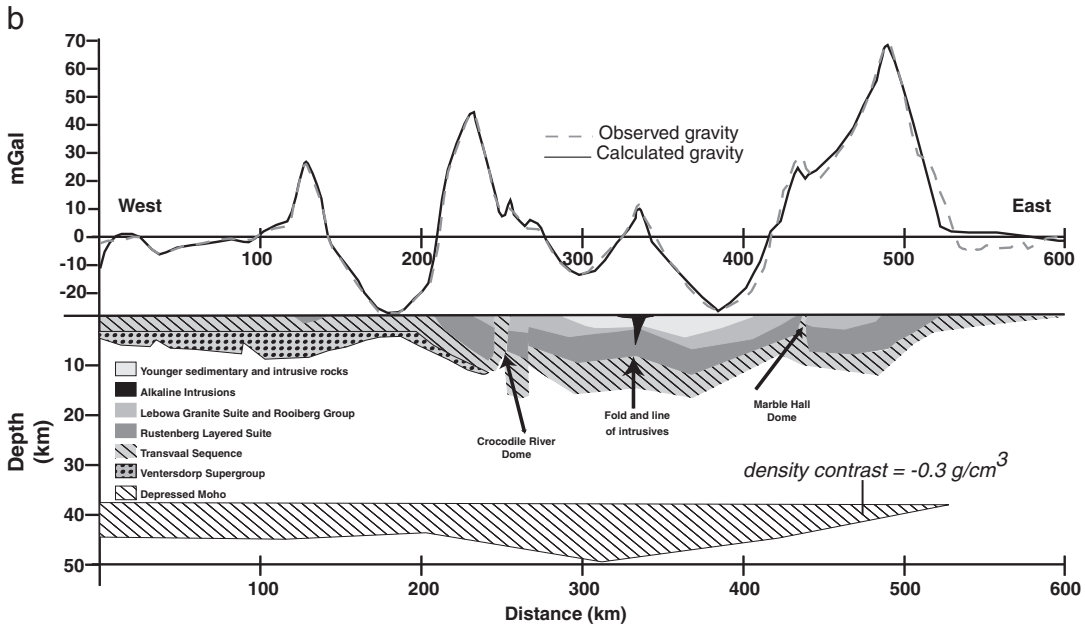
b
mGal
Observed gravity
Calculated gravity
West
East
Depth (km)
Younger sedimentary and intrusive rocks
Alkaline Intrusions
Lebowa Granite Suite and Rooiberg Group
Rustenberg Layered Suite
Transvaal Sequence
Ventersdorp Supergroup
Depressed Moho
Crocodile River Dome
Fold and line of intrusives
Marble Hall Dome
density contrast = -0.3 g/cm3
Distance (km)

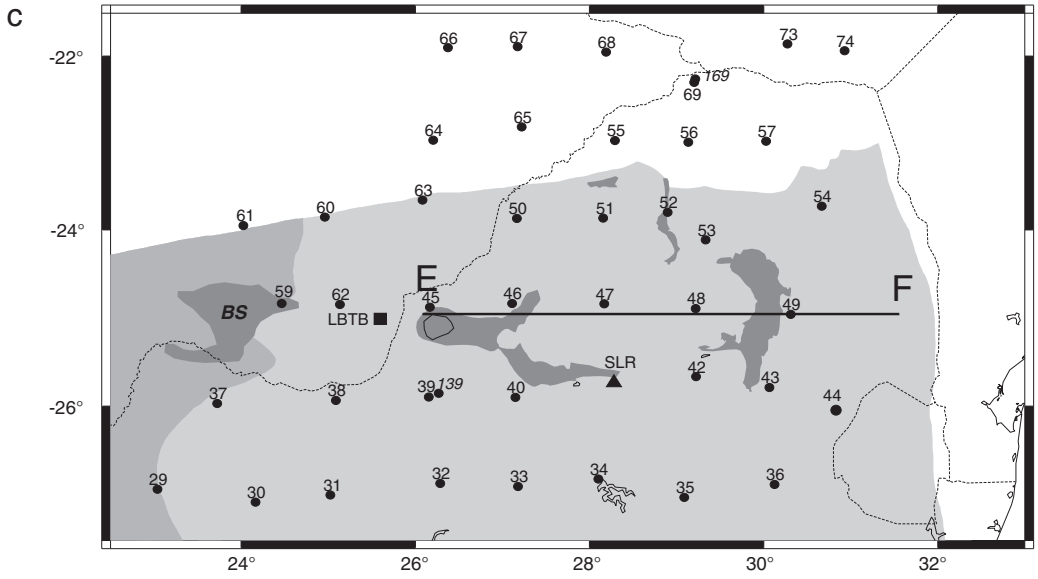
c
BS
LBTB
SLR
E
F
-22°
-24°
-26°
24°
26°
28°
30°
32°

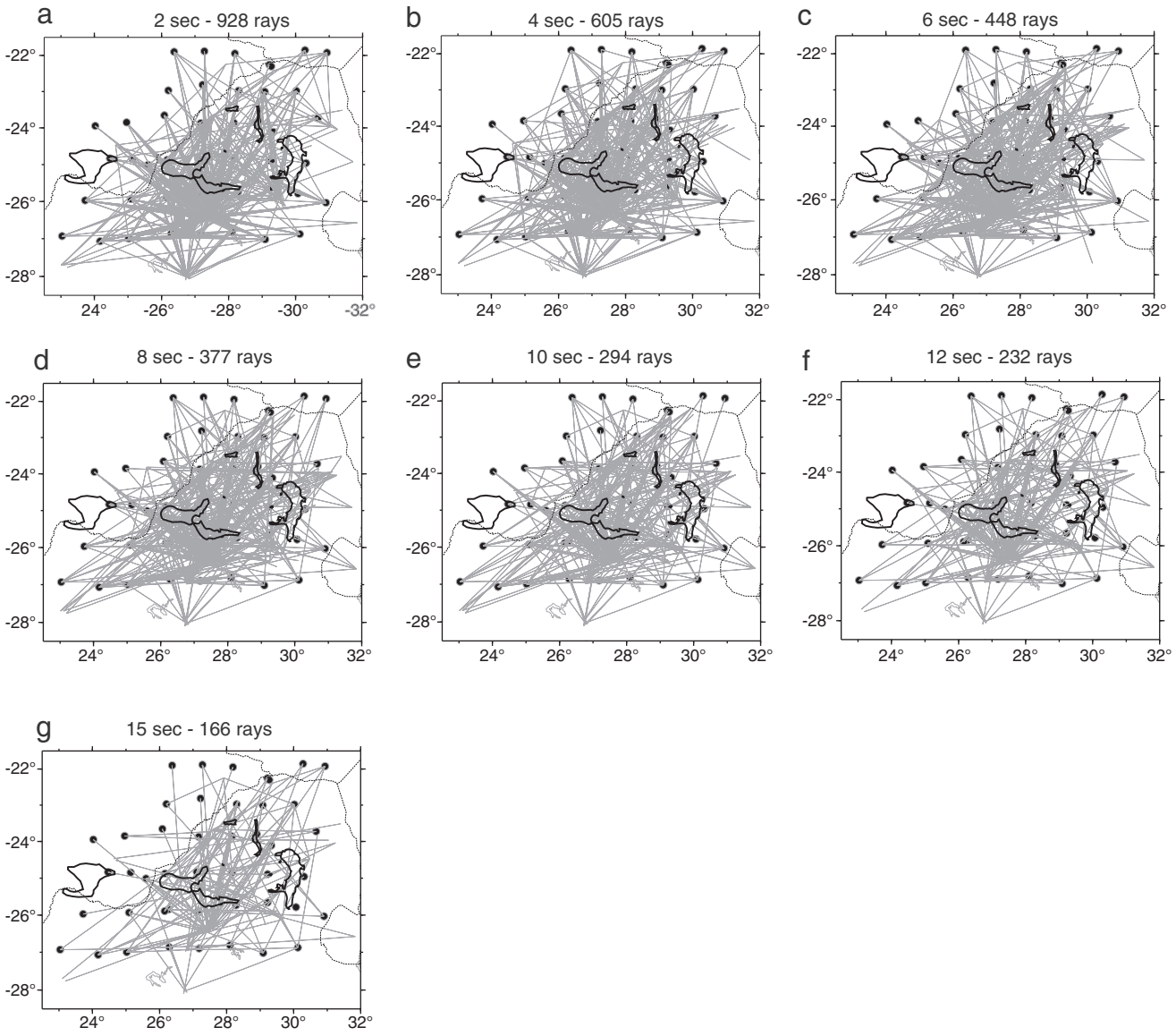

Fig. 3. Raypath maps for periods of 2, 4, 6, 8, 10, 12 and 15 s. Outlines of the BC outcrops are shown with solid black lines. The solid black circles show the position of the stations.

receiver functions were obtained for 16 of these stations (shown in Fig. 1). A total of 100 teleseismic earthquakes were used to compute receiver functions (see Supplemental material), many of them the same as used by Kgaswane et al. (2009).

Receiver functions were computed using the iterative time-domain deconvolution method of Ligorría and Ammon (1999). For each teleseismic event, receiver functions were computed at a frequency band of $f \leq 1.25$ Hz (Gaussian bandwidth of 2.5 s) with a maximum number of 200 iterations. For each station, the receiver functions were binned in ray parameter groups from 0.04 to 0.049 s/km, 0.05 to 0.059 s/km, and 0.06 to 0.069 s/km, and also by backazimuth, and then stacked. The purpose of grouping the receiver functions according to ray parameter is to account for the phase move-out due to varying incidence angles (Cassidy, 1992; Gurrola and Minster, 1998). Fig. 7 shows examples of receiver functions for two stations, illustrating the quality of the data.

2.3. Joint inversion

The joint inversion of receiver functions and surface wave dispersion measurements yields 1-D Vs models of the structure beneath each recording station (Julià et al., 2000, 2003). The method used in this study employs a linearized inversion procedure that minimizes a weighted combination of the L2 norm of the vector residuals corresponding to each data set and a model roughness norm (Ammon et al., 1990). The weighting among the data sets is composed of normalization constants that are helpful in equalizing the contribution of each data set to the overall misfit of the objective function. Each data set is normalized by the number of data points, variances and an influence factor controlling the relative influence of each data set on the inverted 1-D Vs models (Julià et al., 2000). The model vector difference norm helps in stabilizing the inversion procedure by placing smoothness constraints on the resulting 1-D

Fig. 2. a. Meyer and De Beer (1987) gravity model. b. Webb et al. (2004) gravity model. The models in a) and b) have been reproduced from Webb et al. (2004). c. Locations of the SASE (solid circles), GSN (solid square) and SANSN (solid triangle) broadband stations within and surrounding the BC. The profile of the two gravity models is shown by the solid line EF. The area marked BS is the Molopo Farms Complex and represents one of the Bushveld satellites. The background gray-shaded regions show the Kaapvaal Craton. Terrain and political boundaries are shown by dashed black and gray lines, respectively.

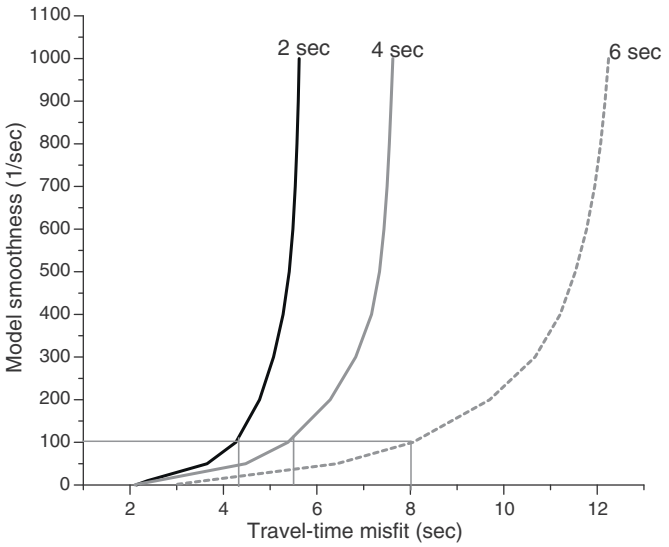

Fig. 4. Trade-off curves of smoothing versus travel-time misfit for periods of 2, 4 and 6 s.

depth-velocity profiles. The model difference norm corresponds to second order differences between adjacent layers (Ammon et al., 1990; Julià et al., 2000). The resulting Vs models are, therefore, a balance between fitting observations, model simplicity and a priori constraints (Julià et al., 2005).

Rayleigh wave group velocities obtained in this study from 2 to 15 s were combined with group velocities from 20 to 60 s from Pasyanos and Nyblade (2007) to create a composite dispersion curve for each station. The dispersion curves were smoothed with a 3-point running average prior to joint inversion with the receiver functions. For each inversion, the influence factor was set to 0.5 and no smoothing was applied, except for stations SA42, SA43 and SA53, for which smoothing parameters slightly greater than or equal to 0.1 were used. An influence factor of 0.5 equalizes the contribution of the combined misfit from each dataset. Fig. 8 shows trade-off curves of (i) waveform misfit versus model roughness and (ii) waveform misfit versus model smoothness for two stations, illustrating that using little, if any, smoothing is justified in the inversions.

The starting model used for the inversions is the PREM model (Dziewonski and Anderson, 1981) modified for continental structure above 60.5 km depth and further modified for the BC upper crust above 10 km depth (Figs. 9 and 10). The model parameterization

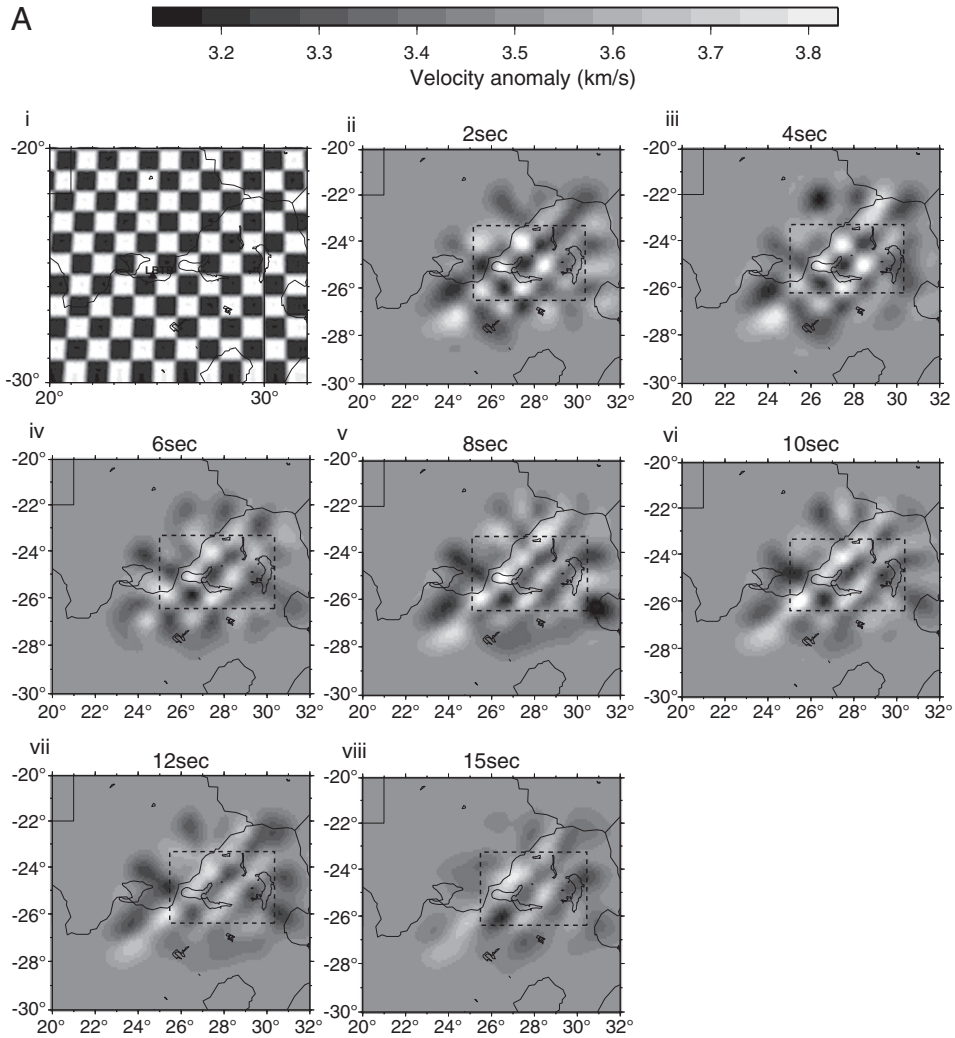

Fig. 5. Resolution tests a. Input (i) and output models (ii–viii) for 100×100 km checkers b. Input (i) and output models (ii–viii) for 125×125 km checkers. The dashed rectangles enclose the area of best resolution.

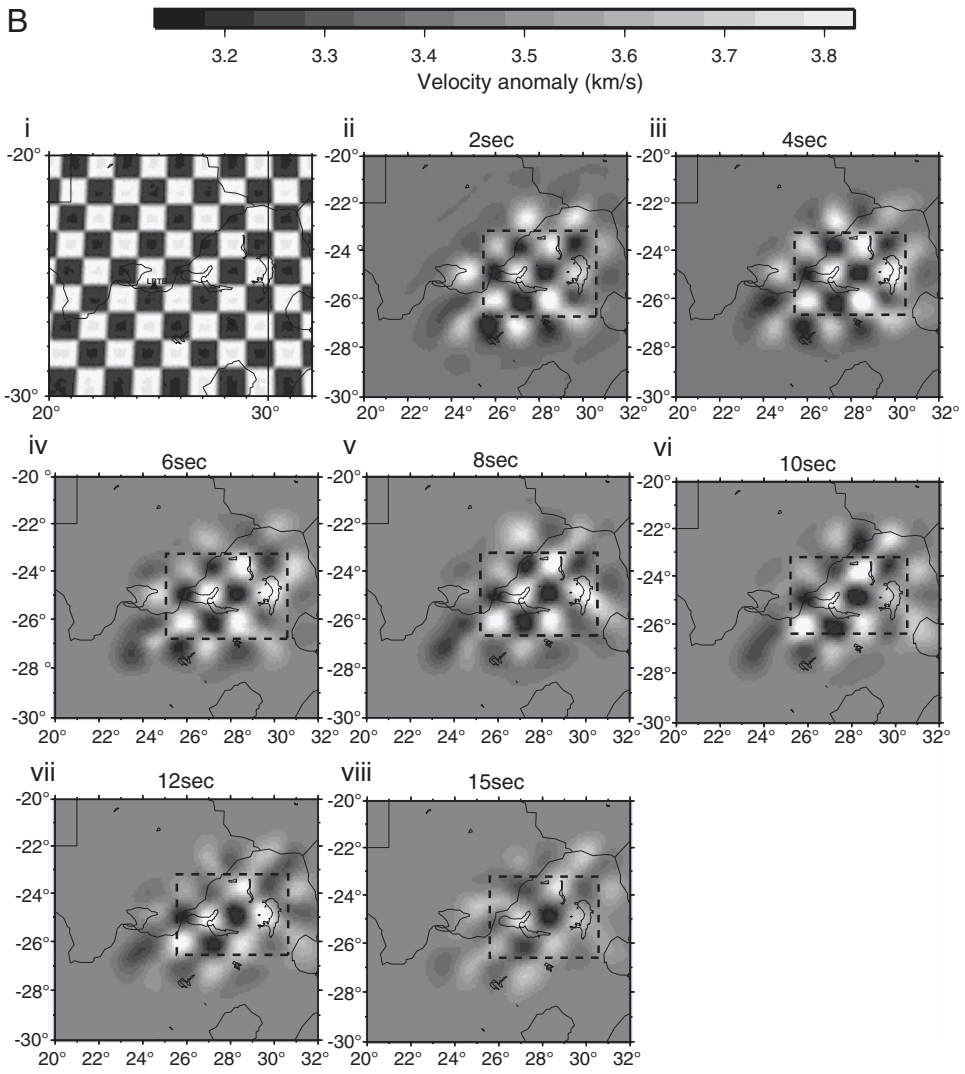

Fig. 5 (*continued*).

consisted of 1-km thick layers to a depth of 10 km, 2.5-km thick layers between depths of 10 to 47.5 km, 5-km thick layers between 47.5 and 242.5 km depth, and 17 to 40-km thick layers below 242.5 km depth. The importance of using 1 km thick layers to parameterize the model in the upper 10 km of the crust is illustrated in Fig. 9, where the fits to the data are compared for two models for station SA47, one with 1-km thick layers and the other with 2 km thick layers. The model with 1-km thick layers fits the receiver function stack better than the model with 2 km thick layers.

To estimate the uncertainties in our velocity model, we follow the approach developed by Julià et al. (2005) for their inversion method, which involves repeatedly performing the inversions using a range of inversion parameters. This may be viewed as an overly simplistic approach, but it is effective in developing a sense of the range of variation of the inverted parameters given the observations and the a priori constraints. As explained by Julià et al. (2000), more sophisticated and statistically rigorous approaches generally require that the observations meet desirable properties, such as being normally distributed, which in general are not satisfied by the data. By following the approach of Julià et al. (2005) of repeatedly performing the inversions with a range of inversion parameters, we obtain an uncertainty of approximately 0.1–0.2 km/s for the velocity in each layer, which translates into an uncertainty of ~2–3 km in the depth of any boundary observed in the model, such as the Moho.

2.3.1. Results

Fig. 10 shows the joint inversion results for all 16 stations, and crustal parameters used in the models are summarized in Table 1 and illustrated in Fig. 11. Many of the stations show a discontinuity where Vs increases from <4.3 km/s to >4.3 km/s, clearly delineating the Moho. For some stations, however, a velocity gradient is observed going from the lower crust into the upper mantle, and for those stations we have placed the Moho at the depth where Vs exceeds 4.3 km/s because velocities ≥4.3 km/s are indicative of mantle lithologies (Christensen, 1996; Christensen and Mooney, 1995). The crustal thicknesses obtained for all 16 stations are similar (i.e., within ~1–3 km) to those reported by Kgaswane et al. (2009).

Fig. 12 shows three profiles across the BC illustrating that the Moho reaches a maximum depth of 45 km in the center of the BC compared to ~37–38 km outside of the BC. In addition to ~5–8 km of crustal thickening, most stations within the BC record a high velocity layer with Vs ≥ 4.0 km/s in the lowermost crust (Table 1). For most of the stations, the thickness of this layer exceeds 5 km, but for a few stations (e.g., station SA50), it is less than 5 km thick.

The joint inversion yields an average Vs of 3.4–3.6 km/s for the crust above 10 km depth for most localities within the BC (Table 1), which is consistent with the upper crustal velocities reported by Yang et al. (2008). However, structural complexities affecting the layering within the upper crust can be inferred for some stations that

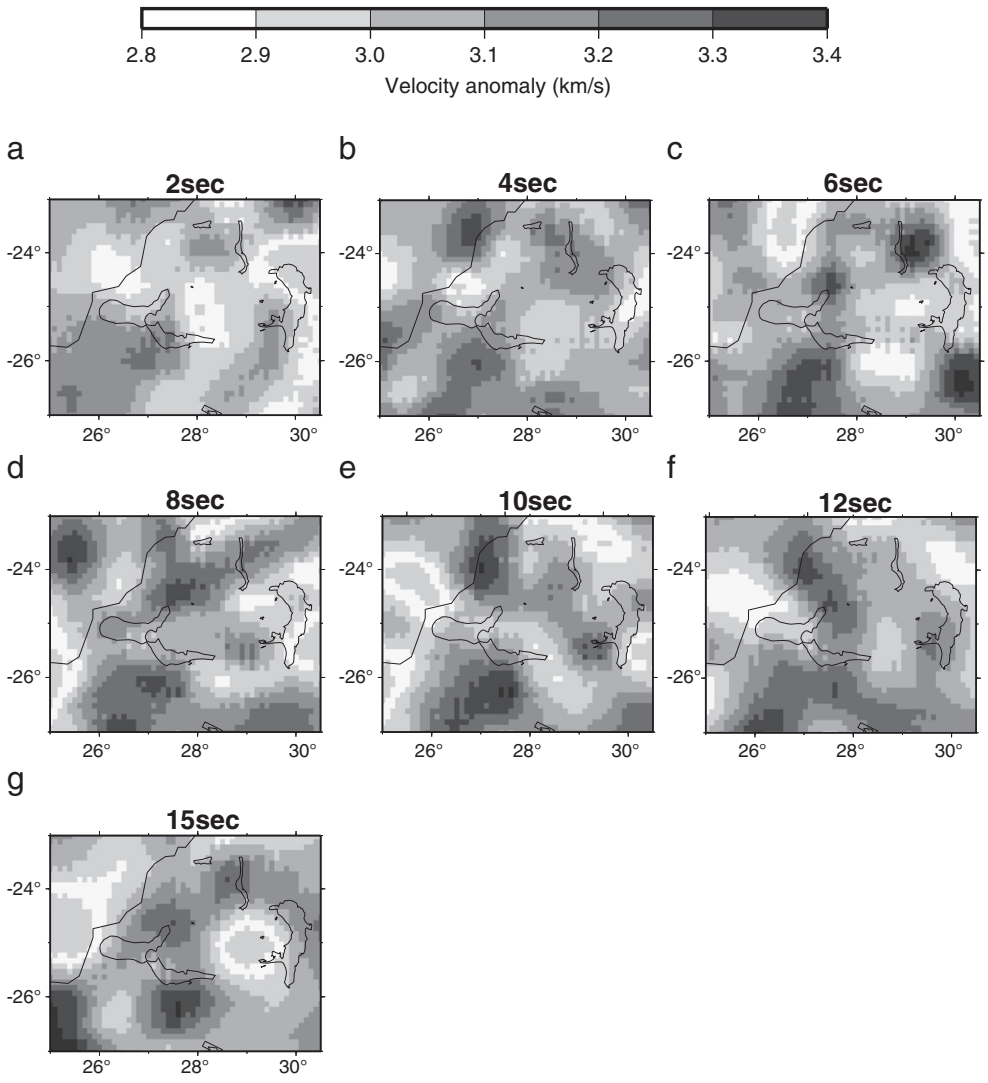

Fig. 6. Rayleigh wave group velocity maps at periods of 2, 4, 6, 8, 10, 12 and 15 s (a–g). The maps show the area within the dashed rectangle in Fig. 5.

record velocities as high as 3.7–3.8 km/s for layers that are only ±2 km thick (i.e., SA47, SA50 and SA53; Fig. 11). In addition, considerable variability in upper crustal structure can be seen for some stations as a function of backazimuth. Station SA47 is a good example, and we examine this variability in detail in Section 3.4.

3. Discussion

To summarize, the main findings of this study are: a) in the center of the BC the crust thickens to a depth of ~45 km (e.g., SA45, SA47, SA48) (Fig. 12) and a substantial portion of the lower crust (greater than 5 km thickness) across the BC consists of high velocity rock (Vs≥4.0 km/s) (Fig. 11), and b) for some stations velocities as high as 3.7–3.8 km/s are found in the upper crust (e.g., SA47, SA50, SA53). For interpreting our results, we convert Vs to density using the empirical Vs–density (ρ) relation from Christensen and Stanley (2003), which was formulated for both crustal and uppermost mantle lithologies at 200 MPa:

$$Vs = 0.0014\rho - 0.4019, \quad (2)$$

Using this equation, a lower crustal Vs of 4.0–4.3 km/s and an uppermost mantle Vs of 4.4–4.6 km/s, yields a density contrast for the crustal "root" of ~−0.2 to −0.3 g/cm^3. Using Eq. (2) and an average Vs of 3.4–3.6 km/s for the top 10 km of the crust, we obtain an average density for the upper crust of 2.7–2.9 g/cm^3. For upper crustal layers with Vs > 3.6 km/s, we obtain densities > 2.9 g/cm^3, which are consistent with the presence of mafic lithologies (Christensen and Stanley, 2003). These findings and density estimates can be used to evaluate the "dipping-sheet" and "continuous-sheet" models for the BC.

3.1. "Dipping-sheet" model

As discussed in the Introduction, the "dipping-sheet" model by Meyer and De Beer (1987) has a gap between the eastern and western limbs and no compensation at the Moho for the dense upper crustal layers (Fig. 2a). This model is not consistent with our findings of crustal thickening in the center of the BC, high Vs layers (Vs≥4.0 km/s) in the lowermost part of the crust (≥40 km), or high upper crustal densities beneath the center of the BC. Therefore, this model is not favored.

3.2. "Continuous-sheet" model

The "continuous-sheet" model by Webb et al. (2004) (Fig. 2b) proposes the presence of continuous mafic layering in the upper crust across the central region of the BC connecting the eastern and

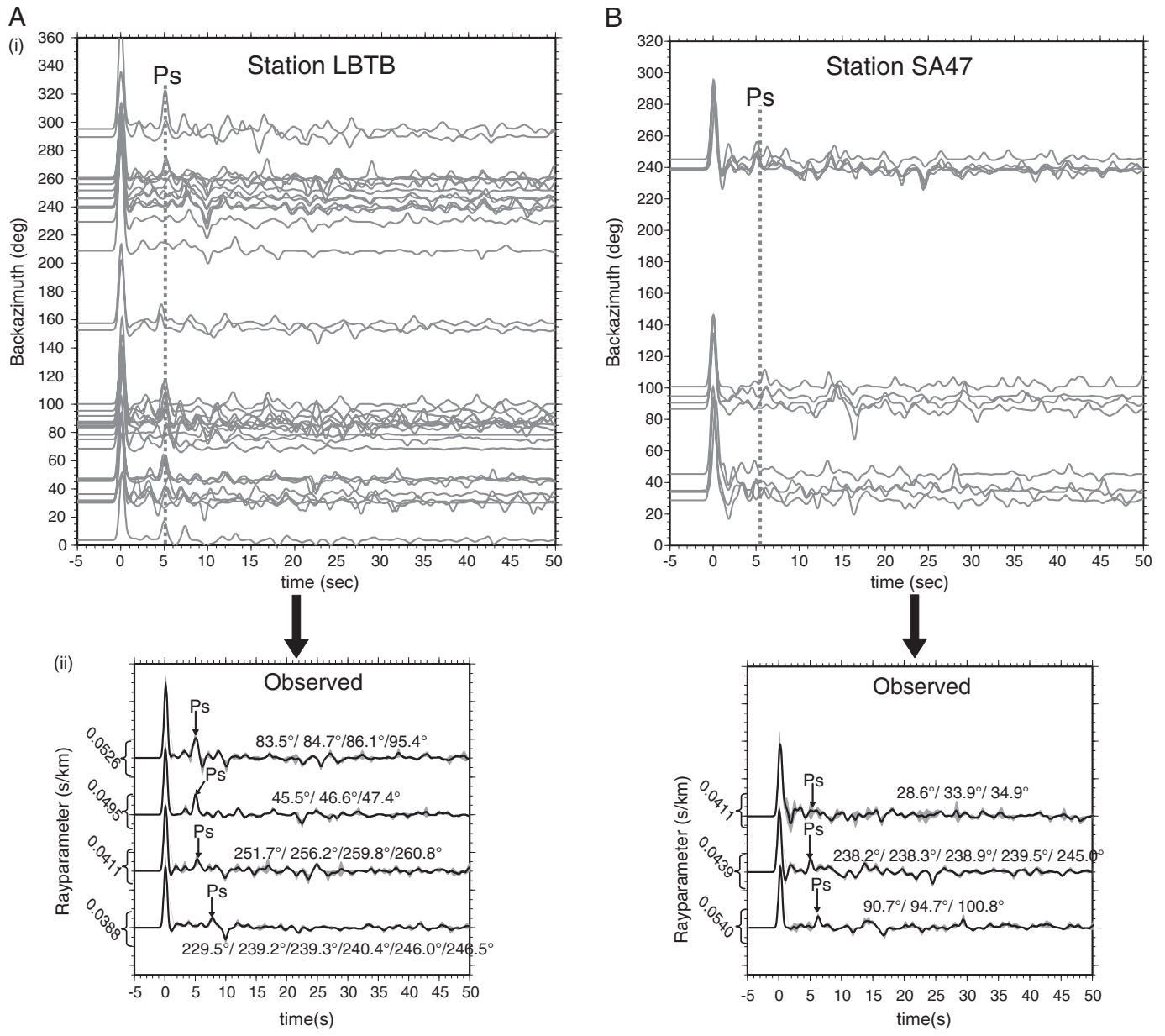

Fig. 7. Receiver functions at stations LBTB and SA47 (columns A and B, respectively). (i) Individual receiver functions for each station. The dashed gray lines show the theoretical arrival time of the Moho converted phase (Ps) for the crustal thicknesses and average crustal Vs for stations LBTB and SA47 reported in Table 1. The theoretical arrival times were computed using the joint inversion code and assuming the PREM model. (ii) Stacked receiver functions grouped according to ray parameter bins and backazimuth. The gray shading around the observed receiver functions shows 1σ error bounds.

western limbs of the BC. The model also includes isostatic compensation of the mafic layering by a thickened crust in the center of the BC, extending to a depth of ~50 km. In this model, a density contrast of 0.3 g/cm^3 for each of the upper crust mafic layers is used along with a density contrast of −0.3 g/cm^3 for the crustal root (>38 km depth).

Our results show that the crust has a thickness of ~45 km beneath the center of the BC (Fig. 12), consistent with, but somewhat thinner than, the lower crustal structure in the Webb et al. (2004) model. The Webb et al. (2004) model assumes an average density of 2.9 g/cm^3 for the structure above 10 km depth in the center of the BC, which is equivalent to a Vs of 3.65 km/s using the relation in Eq. (2). The Vs models (Figs. 10 and 11) for some stations show Vs > 3.65 km/s within upper crustal layers, as noted previously, and therefore our results are broadly consistent with the upper crustal structure in the Webb et al. (2004) model.

3.3. Refinement of the Webb et al. (2004) density model

Fig. 13 shows a revised density model that includes several adjustments to the Webb et al. (2004) model to make it consistent with our seismic models. Similar to Webb et al. (2004), a background density of 2.7 g/cm^3 was used for the bulk crust as well as the same density contrasts for the upper crustal layers (see Fig. 13). Based on the seismic results, we assume a density of 3.3–3.4 g/cm^3 for the uppermost mantle. For the crustal "root" (>37.5 km depth), a density contrast of −0.2 g/cm^3 was used instead of the −0.3 g/cm^3 density contrast used by Webb et al. (2004). After changing the structure and density of the crustal "root", we then adjusted the thickness of the upper crustal layers to obtain a good fit to the gravity data.

In the revised density model (Fig. 13), the mafic layering in the upper crust remains continuous across the BC with a maximum

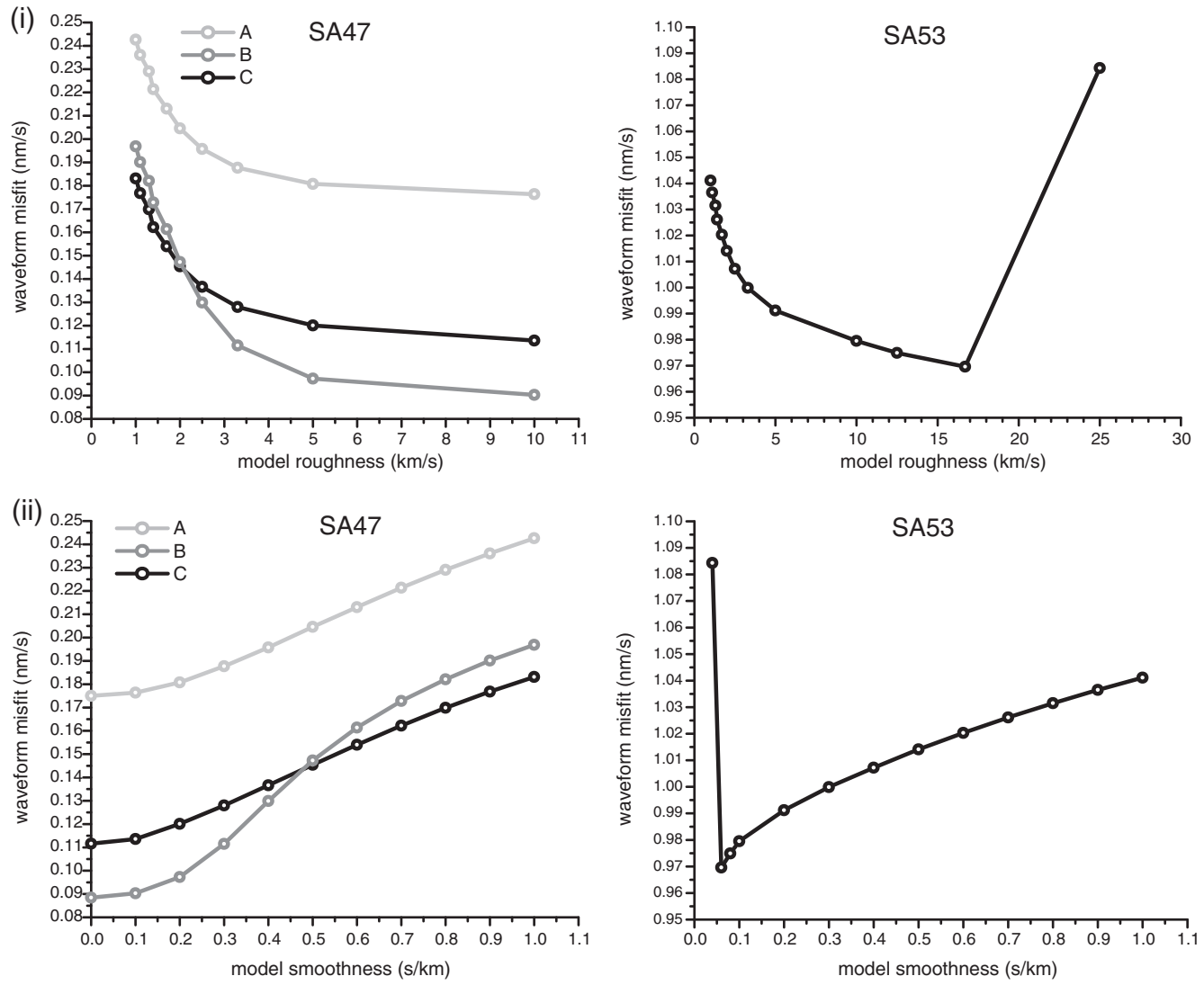

Fig. 8. Plots of waveform misfit as a function of model roughness and model smoothness (i and ii, respectively) for stations SA47 and SA53. Labels A, B, C for station SA47 refer to the three receiver function stacks for this station shown in Fig. 10.

thickness of 4–5 km, similar to Webb et al. (2004). However, the layers of the Transvaal Sequence and younger sediments in the center of the BC are somewhat thinner than those reported by Webb et al. (2004). This illustrates that to accommodate the difference in crustal thickness between the Webb et al. (2004) model and our seismic results, only minor adjustments are required to the Webb et al. (2004) model.

3.4. Structural complexity in the upper crust

Although our results are in general agreement with Webb et al. (2004) suggesting the presence of mafic lithologies beneath the center of the BC, our results also indicate that there is a considerable structural complexity within the upper crust, much more than is shown in either the Webb et al. (2004) model or in Fig. 13. We illustrate this by carefully examining the receiver functions for station SA47, which is located near the center of the BC (Fig. 1). The geology immediately around station SA47 is shown in Fig. 14. Plotted on this figure are average Ps conversion points at 5 km depth for the three receiver function stacks for SA47 shown in Fig. 10. The Vs profile for SA47 at backazimuth (a) in Fig. 11 corresponds to the conversion point at A in Fig. 14, and similarly the Vs profiles at backazimuths (b) and (c) correspond to conversion points B and C, respectively. Fig. 14 shows an overthrust just to the south of station SA47, resulting in a complicated anticlinal structure with the receiver functions likely sampling different lithologies (i.e., granites, sandstones, quartzites) depending on backazimuth and depth.

In Fig. 15, the three receiver function stacks for SA47 are modeled to ascertain the effect of upper crustal structure on the waveforms. The synthetic receiver functions in the first column of Fig. 15 were obtained from the joint inversion, whereas those in the second and third columns were generated using a code based on a reflection matrix method by Kennett (1983). For reference, the first column of receiver functions shows the fit between observed and synthetic receiver functions for the models obtained from the joint inversion. The first prominent phase after the direct P arrival within the first 2 s is labeled P1, and is the primary arrival resulting from upper crustal structure. There is a considerable variability in this phase between the three receiver function stacks. For stack (a), the phase is characterized by a large down-swing with a peak amplitude at 1.8 s. For stack (b), the phase is characterized by a large down-swing with a peak amplitude at 1.0 s. And for stack (c), the phase is characterized by a small down-swing with a peak amplitude around 1.7 s. The Ps conversion from the Moho is also labeled on each stack.

In the second column, we show synthetic receiver functions for a velocity model that contains the velocity layering in the upper

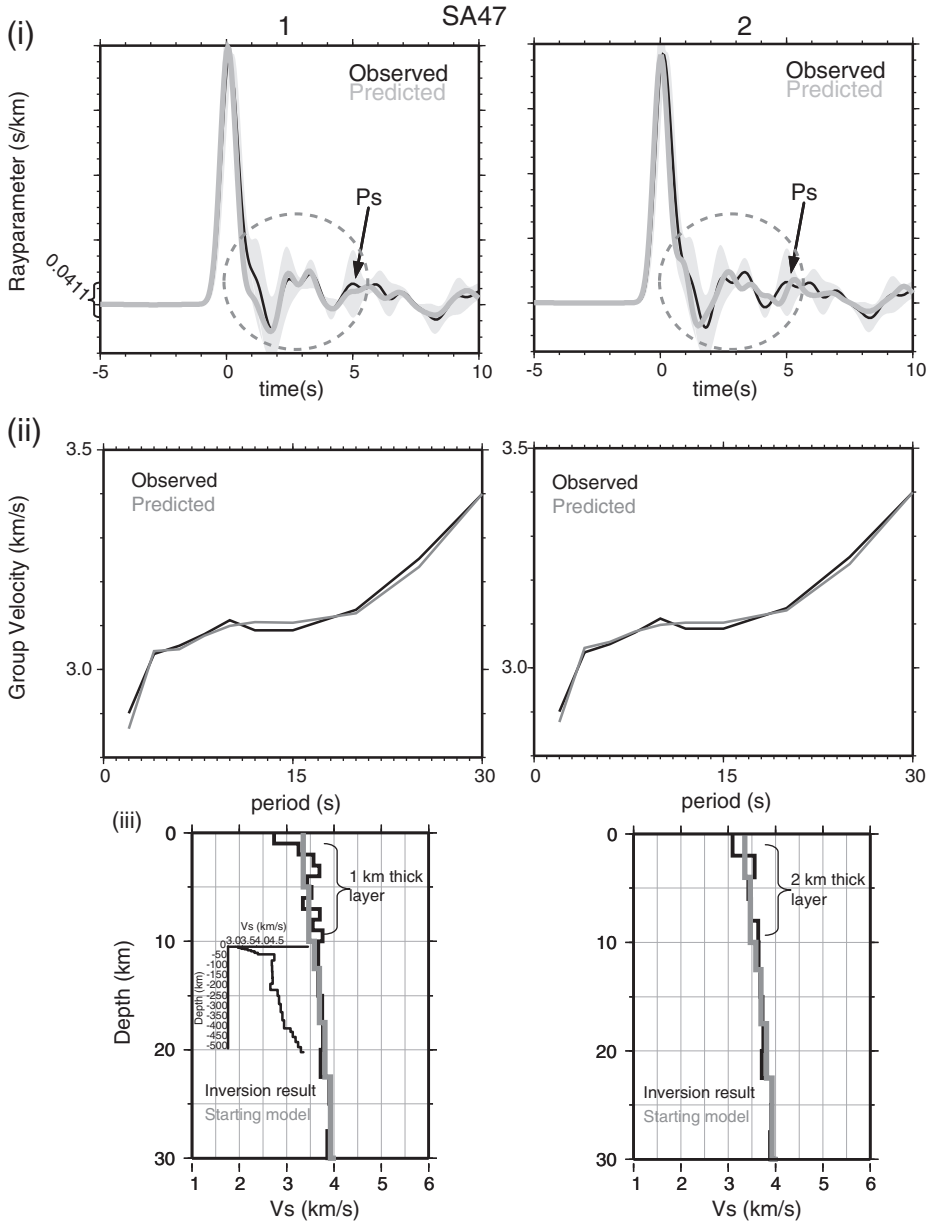

Fig. 9. Diagram for station SA47 illustrating the improved fit to the receiver functions by using 1 km thick layers (column 1) in the top 10 km of the model versus 2 km thick layers (column 2). The Ps conversion from the Moho is labeled "Ps", and the gray shading around the observed receiver function shows 1σ error bounds.

10 km of the crust from the joint inversion models (shown at far left in Fig. 15), and a half space beneath it with a velocity of 3.6 km/s. A comparison between the synthetic and actual receiver functions illustrates that the P1 phase does indeed originate from structure (i.e. thrusted zone) within the top 10 km of the crust.

To isolate which layers within the top 10 km of the crust influence the P1 phase the most, in the third column we show two synthetic receiver functions with altered upper crustal layering (structure below 10 km is the same as in the joint inversion models). In the first one (dotted line), the low velocity layer in the top 1 km of the model is removed (i.e., the topmost velocity is increased to the velocity in the layer just below it). A comparison of the receiver function fits shows that the earlier arriving P1 phase in stack (b) is changed significantly (effectively removed), but the fits for stacks (a) and (c) are essentially unchanged, indicating that the later arriving P1 phases in those stacks might be influenced by deeper structure. In the second case (gray line), the velocity structure in the top 10 km is set to a uniform 3.4 km/s, thus removing all of the higher velocity layering in the top 10 km of the crust seen in the joint inversion models. Even though the velocity models (gray lines) in the third column have been set to a uniform 3.4 km/s in the top 10 km of the crust, the corresponding receiver functions are different because of influences from structures below 10 km depth. In this case, the P1 phase in stacks (a) and (c) is significantly altered, indicating that the higher velocity layering between 1 and 10 km depth in the joint inversion model is required to fit the P1 phase.

Our modeling shows that the receiver function stacks from two of the three backazimuths (stacks a and c) require higher velocity layers (i.e., Vs of 3.7–3.8 km/s) in the upper crust to obtain a good fit, as compared to stack (b). These results suggest that the mafic layering may be better developed to the east and northeast of station SA47 than to the southwest, and hence the upper crustal structure is not as uniform as illustrated by the gravity models (Fig. 13 and Webb et al., 2004). The non-uniformity could potentially be a characteristic of much of the central areas of the BC. The non-uniformity could either be entirely or partially associated with the diapirism and

metamorphism and associated structural complexity triggered by the emplacement of the BC (Uken and Watkeys, 1997).

Fig. 1 shows the position of some of the domes associated with diapirism triggered by high thermal gradients at the base of the BC. According to Uken and Watkeys (1997), the domes were produced by gravitational loading and heating of the sedimentary rocks of the Transvaal Supergroup below the floor of the BC. For areas where temperatures were above 550 °C, these floor rocks became unstable and diapirically rose into the overlying units of the RLS. Although the domes are best exposed towards the margins of the BC, as shown in Fig. 1, the diapirism of floor rocks into the overlying RLS could be widespread across the center of the BC, assuming that diapirism was generally driven by thermal destabilization of low density rocks of the Transvaal Sequence (Uken and Watkeys, 1997).

Thermally-driven diapirism as proposed by Uken and Watkeys (1997) may not be the only source of structural complexity affecting the BC. Field, petrographic and $^{40}Ar/^{39}Ar$ data presented by Alexandre et al. (2006, 2007) for Pretoria Group rocks (west of Pretoria) strongly support a ~2040 Ma episode of intracratonic crustal shortening marked by folding, thrusting and lower greenschist facies metamorphism best observed in the broad area between Pretoria, the village of Magaliesburg, and the Cradle of Humankind (cf. Andreoli, 1988a, 1988b). Further evidence for this so-called "Transvaalide" tectonic–metamorphic event, tentatively linked to coeval reactivation of the Central Zone in the Limpopo Belt, was also identified in the Malip River–Pilgrim's Rest areas, close to the NE and E margin of the BC respectively (cf. Alexandre et al., 2006; Harley and Charlesworth, 1994).

4. Summary

The 1-D shear wave velocity models have been obtained for the BC crust by jointly inverting high-frequency receiver functions and Rayleigh wave group velocities for 16 broadband seismic stations spanning the BC. The 1-D shear wave velocity models show that, 1) there is ~5–8 km crustal thickening beneath the center of the BC, 2) shear wave velocities reach 4.0 km/s or higher over a significant portion of the lower crust, and 3) there are upper crustal layers beneath the center of the BC with shear wave velocities high enough (Vs > 3.65 km/s) to indicate the presence of mafic lithologies. These findings are consistent with the "continuous-sheet" model (e.g., Webb et al., 2004) for the BC. However, detailed modeling of receiver function stacks for station SA47 in the center of the BC shows that the upper crustal structure varies considerably around the station, indicating that the structure of the BC at depth is locally complicated. This inhomogeneity

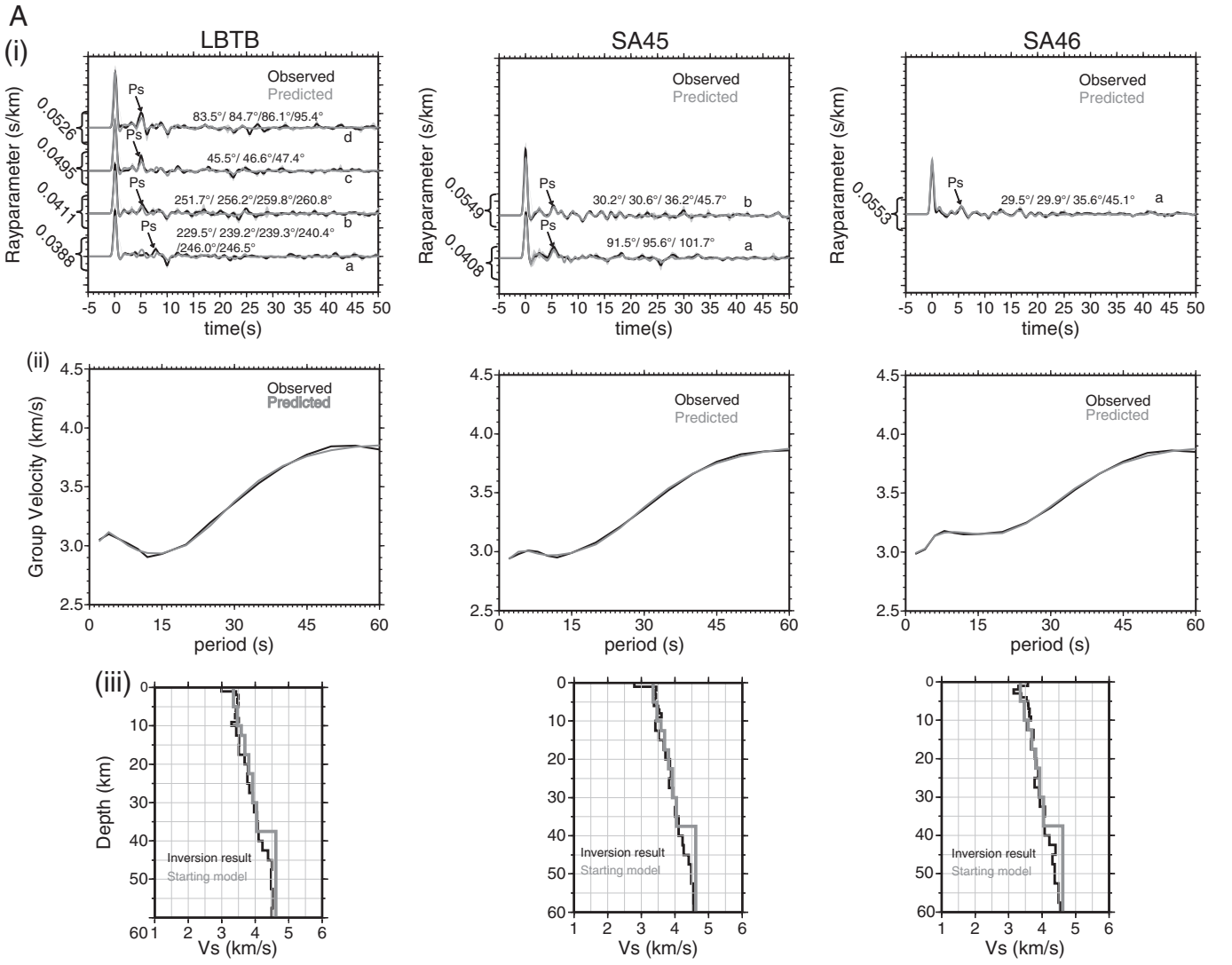

Fig. 10. Joint inversion results for the 16 stations (i) Observed (black curves) and predicted (gray curves) receiver functions with 1σ error bounds shown with gray shading around the observed receiver functions. The backazimuths of the receiver functions within each stack are shown on top. (ii) Observed (black curves) and predicted (gray curves) group velocities. (iii) Shear wave velocity models obtained from the joint inversion.

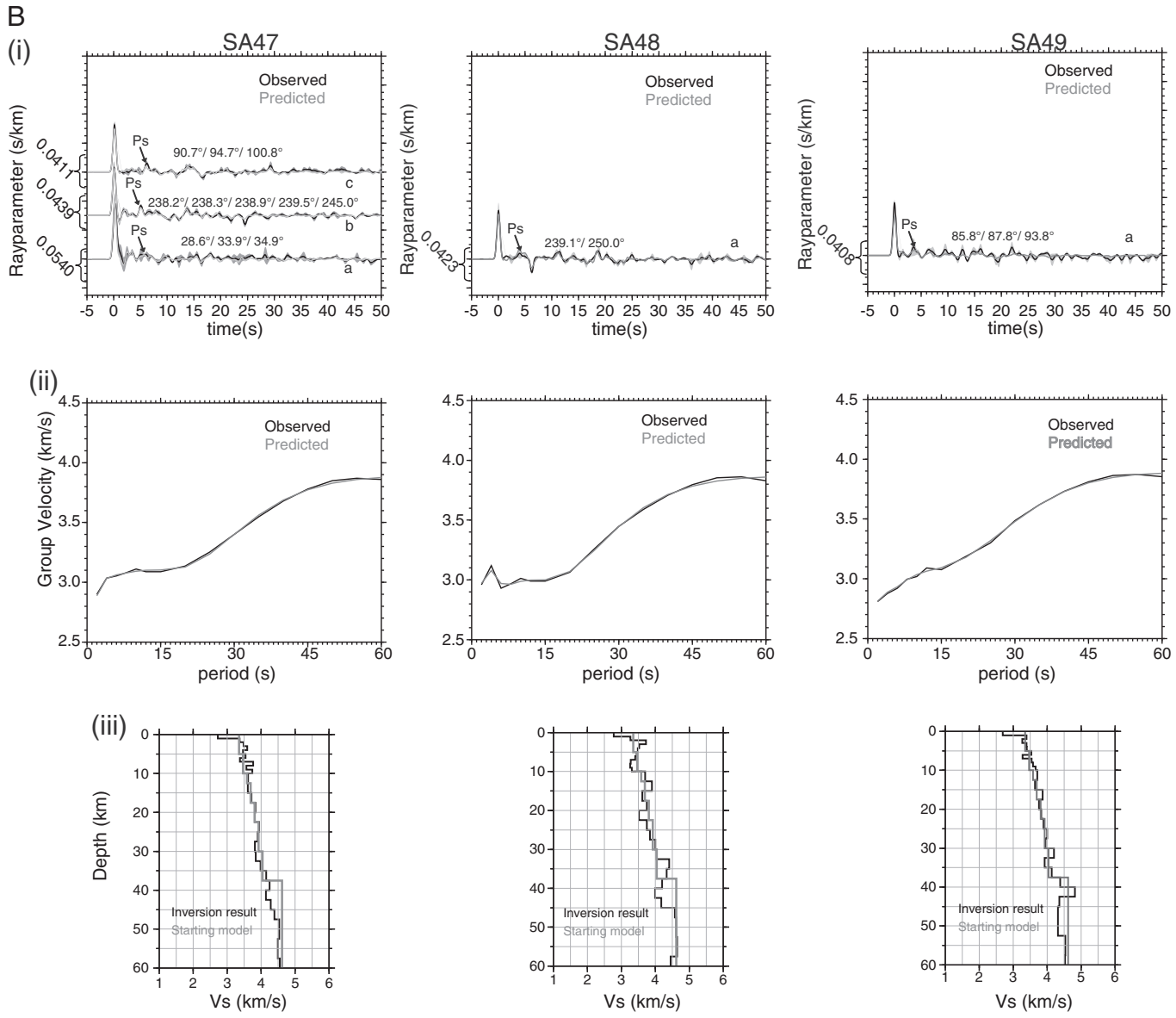

Fig. 10 (*continued*).

may be the result of thermal diapirism triggered by the emplacement of the BC at ~2060 Ma, or thermal and tectonic reactivation produced by a ~2040 Ma intraplate event.

Supplementary data to this article can be found online at http://dx.doi.org/10.1016/j.tecto.2012.06.003.

Acknowledgments

We would like to thank Charles Ammon for the use of his inversion code, Yongcheol Park for assistance with the computer codes, Tarzan Kwadiba for the additional catalog of earthquakes used for the group velocity measurements and all those who assisted with the Southern African Seismic Experiment. Discussions with Marco Andreoli have provided further clarity to the interpretation of the results of this study. Two anonymous reviewers provided comments that helped to improve this manuscript. E.K. would like to acknowledge support from the Council for Geoscience and the AfricaArray program and R.J.D. acknowledges support from the DST/NRF South African Research Chair program. This research has been supported by the National Science Foundation (grants EAR 0440032 and OISE 0530062), the AfricaArray program and the South African National Research Foundation.

References

Alexandre, P., Andreoli, M.A.G., Jamison, A., Gibson, R.L., 2006. $^{40}Ar/^{39}Ar$ age constraints on low-grade metamorphism and cleavage development in the Transvaal Supergroup (Central Kaapvaal craton, South Africa): implications for the tectonic setting of the Bushveld igneous complex. South African Journal of Geology 109, 393–410.

Alexandre, P., Andreoli, M.A.G., Jamison, A., Gibson, R.L., 2007. Response to the comment by Reimold et al. on $^{40}Ar/^{39}Ar$ age constraints on low-grade metamorphism and cleavage development in the Transvaal Supergroup (central Kaapvaal Craton, South Africa): implications for the tectonic setting of the Bushveld Igneous Complex (South African Journal of Geology, 109, 393–410), by Alexandre et al. (2006). South African Journal of Geology 110, 160–162.

Ammon, C.J., 2001. Notes on Seismic Surface-Wave Processing, Part 1, Group Velocity EstimationSaint Louis University, version 3.9.0. , http://eqseis.geosc.psu.edu/~cammon2001.

Ammon, C.J., Randall, G.E., Zandt, G., 1990. On the nonuniqueness of receiver function inversions. Journal of Geophysical Research 95, 15303–15318, http://dx.doi.org/10.1029/JB095Ib10p15303.

Andreoli, M.A.G., 1988a. The discovery of a hidden and strange African orogeny: the Transvaalide Fold Belt. Tectonic Division, Geol. Soc. S. Africa, Abstracts Vol. 4th Annual Conference, Silverton, 25 February 1988, pp. 1–2.

Andreoli, M.A.G., 1988b. Evidence for thrust tectonics in the Transvaal Sequence based on geophysical profiles. Ext. Abstracts Geocongress'88, Geol Soc. S. Afr., Durban, South Africa, pp. 3–6.

Biesheuvel, K., 1970. An interpretation of a gravimetric survey in the area west of Pilanesburg in the western Transvaal. Geological Society of South Africa, Special Publications 1, 266–282.

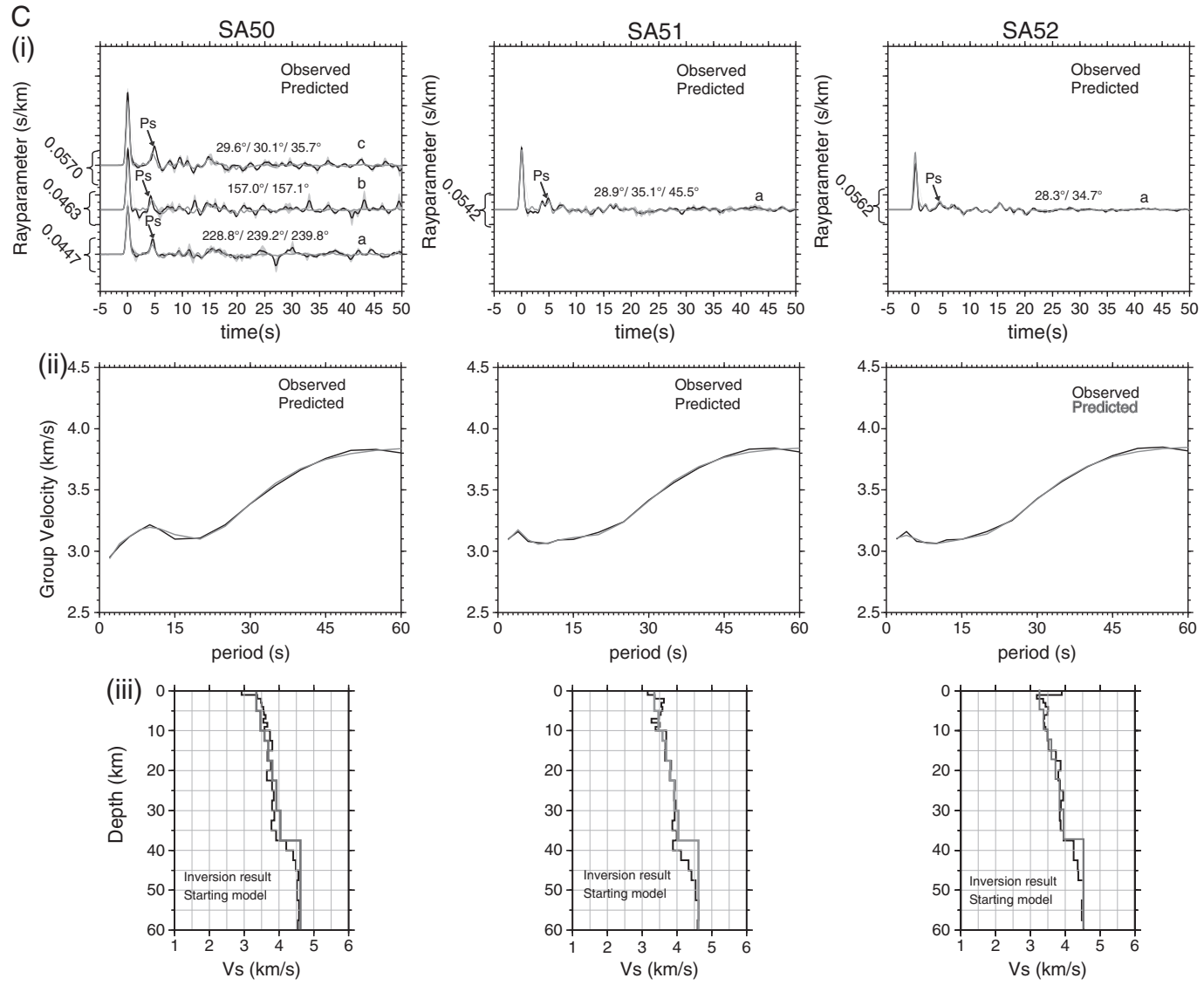

Fig. 10 (*continued*).

Carlson, R.W., Grove, T.L., De Wit, M.J., Gurney, J.J., 1996. Program to study crust and mantle of the Archean Craton in southern Africa. EOS, Transactions, American Geophysical Union 77 (29), 273–277, http://dx.doi.org/10.1029/96EO00194.

Cassidy, J.F., 1992. Numerical experiments in broad-band receiver function analysis. Bulletin of the Seismological Society of America 82, 1453–1474.

Cawthorn, R.G., Webb, S.J., 2001. Connectivity between the western and eastern limbs of the Bushveld Complex. Tectonophysics 300, 195–2009.

Cawthorn, R.G., Cooper, G.R.J., Webb, S.J., 1998. Connectivity between the western and eastern limbs of the Bushveld Complex. South African Journal of Geology 101, 291–298.

Cawthorn, R.G., Eales, H.V., Walraven, F., Uken, R., Watkeys, M.K., 2006. The Bushveld Complex. In: Johnson, M.R., Anhaeusser, C.R., Thomas, R.J. (Eds.), The Geology of South Africa. : Geological Society of South Africa. Johannesburg/Council for Geoscience, Pretoria, pp. 261–281.

Christensen, N.I., 1996. Poisson's ratio and crustal seismology. Journal of Geophysical Research 101, 3139–3156.

Christensen, N.I., Mooney, W.D., 1995. Seismic velocity structure and composition of the continental crust: a global view. Journal of Geophysical Research 100, 9761–9788.

Christensen, N.I., Stanley, D., 2003. Seismic velocities and densities. In: Lee, W.H.K., Kanamori, H., Jennings, P.C., Kisslinger, C. (Eds.), International Handbook of Earthquake and Engineering, 81B, pp. 1587–1594.

Claerbout, J.F., 1992. Earth Soundings Analysis: Processing Versus Inversion. Blackwell Scientific Publications, Boston, MA. 304 pages.

Cousins, C.A., 1959. The structure of the mafic portion of the Bushveld Igneous Complex. Transactions of the Geological Society of South Africa 62, 179–189.

Du Plessis, A., Kleywegt, R.J., 1987. A dipping sheet model for the mafic lobes of the Bushveld Complex. South African Journal of Geology 90, 1–6.

Du Toit, A.L., 1954. The Geology of South Africa. Oliver and Boyd, Edinburgh, U.K. 539 pp.

Dziewonski, A.M., Anderson, D.L., 1981. Preliminary reference Earth model. Physics of the Earth Planetary Interiors 25, S.297–S.356.

Dziewonski, A., Bloch, S., Landisman, L., 1969. A technique for the analysis of transient seismic signals. Bulletin of the Seismological Society of America 59, 427–444.

Eglington, B.M., Armstrong, R.A., 2004. The Kaapvaal Craton and adjacent orogens, southern Africa: a geochronological database and overview of the geological development of the Craton. South African Journal of Geology 107, 13–32.

Gurrola, H., Minster, J.B., 1998. Thickness estimates of the uppermantle transition zone from bootstrapped velocity spectrum stacks of receiver functions. Geophysical Journal International 133, 31–43, http://dx.doi.org/10.1046/j.1365-246X.1998.1331470.x.

Hall, A.L., 1932. The Bushveld Igneous Complex of the central Transvaal. South African Geological Survey Memoir, 28. Pretoria, 560 pp.

Harley, M., Charlesworth, E.G., 1994. Structural development and controls to epigenetic, mesothermal gold mineralization in the Sabie–Pilgrim's Rest goldfield, eastern Transvaal, South Africa. Exploration and Mining Geology 3, 231–246.

Hatton, C.J., Schweitzer, J.K., 1995. Evidence for synchronous extrusive and intrusive Bushveld magmatism. Journal of African Earth Sciences 21, 579–594.

Jorissen, 1904. On the occurrence of the Dolomite and Chert Series in the Rustenburg district. Transvaal Geological Society of South Africa 7, 30–38.

Julià, J., Ammon, C.J., Hermann, R.B., Correig, A.M., 2000. Joint inversion of receiver functions and surface-wave dispersion observations. Geophysical Journal International 143, 99–112.

Julià, J., Ammon, C.J., Hermann, R.B., 2003. Lithospheric structure of the Arabian Shield from the joint inversion of receiver functions and surface-wave group velocities. Tectonophysics 371, 1–21.

Julià, J., Ammon, C.J., Nyblade, A.A., 2005. Evidence for mafic lower crust in Tanzania, East Africa from joint inversion of receiver functions and Rayleigh wave dispersion velocities. Geophysical Journal International 162, 555–569.

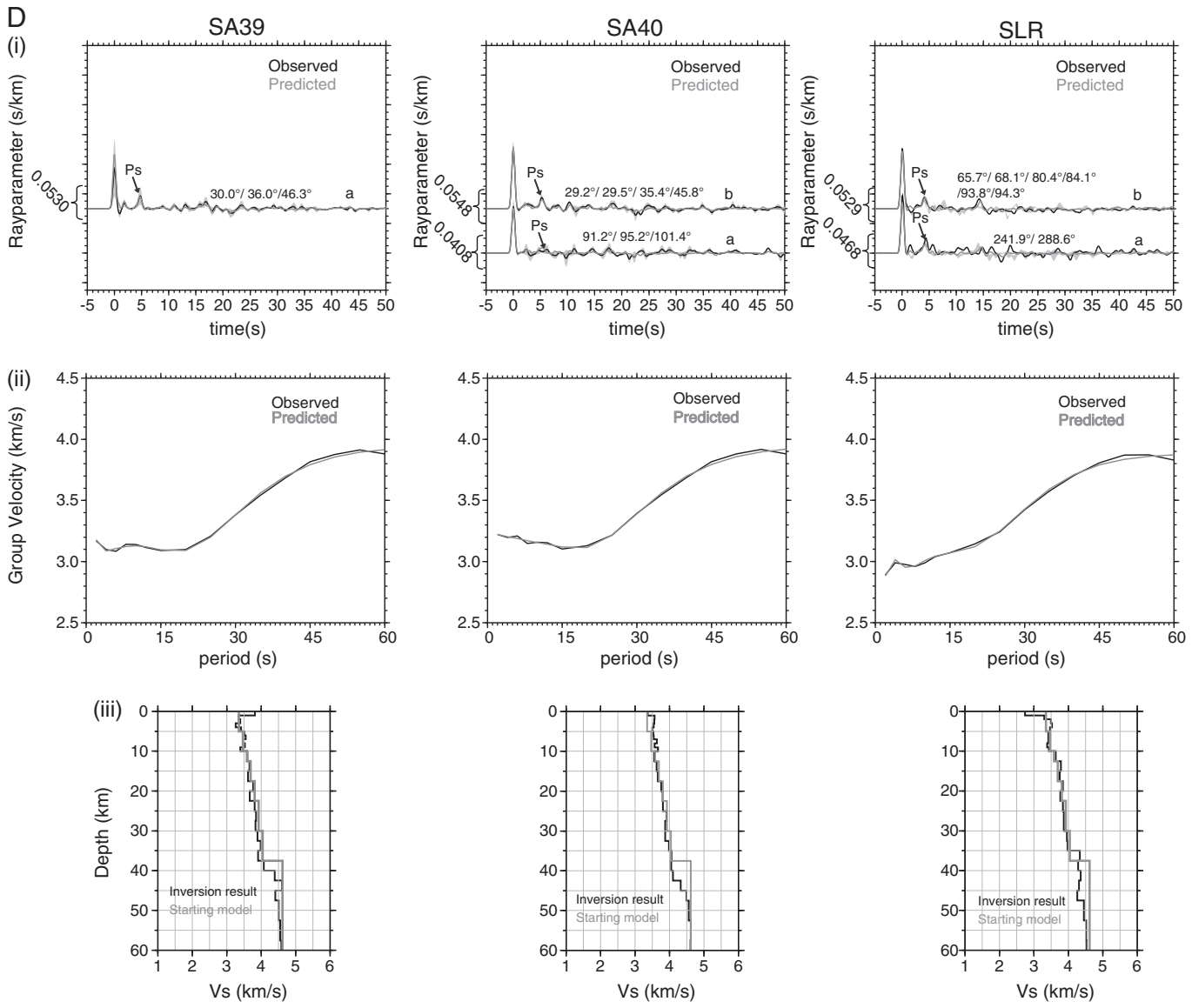

Fig. 10 (*continued*).

Keilis-Borok, V.I., 1989. Seismic Surface Waves in a Laterally Inhomogeneous Earth. Kluwer Academic Publishers, Dordrecht.

Kennett, B.L.N., 1983. Seismic Wave Propagation in Stratified Media. Cambridge University Press, Cambridge.

Kgaswane, E.M., Nyblade, A.A., Julià, J., Dirks, P.H.G.M., Durrheim, R.J., Pasyanos, M.E., 2009. Shear wave velocity structure of the lower crust in southern Africa: evidence for compositional heterogeneity within Archaean and Proterozoic terrains. Journal of Geophysical Research 114, B12304, http://dx.doi.org/10.1029/2008JB006217.

Levshin, A., Ratnikova, L., Berger, J., 1992. Peculiarities of surface-wave propagation across central Asia. Bulletin of the Seismological Society of America 82, 2464–2493.

Ligorría, J.P., Ammon, C.J., 1999. Iterative deconvolution and receiver function estimation. Bulletin of the Seismological Society of America 89, 1359–1400.

Mellor, E.T., 1906. The geology of the central portion of the Middelburg district. Annual Report of the Geological Survey of Transvaal 55–71.

Meyer, R., De Beer, J.H., 1987. Structure of the Bushveld Complex from resistivity measurements. Nature 325, 610–612.

Molengraaff, G.A.F., 1901. Geologie de la Republique S. Africaine. Bulletin of the Geological Society of France 1, 13–92.

Molengraaff, G.A.F., 1902. Vice President's address. Transvaal Geological Society of South Africa 5, 69–75.

Molyneux, T.G., Klinkert, P.S., 1978. A structural interpretation of part of the eastern mafic lobe of the Bushveld Complex and its surrounds. Transactions of the Geological Society of South Africa 81, 359–368.

Nair, S.K., Gao, S.S., Kelly, H.L., Silver, P.G., 2006. Southern African crustal evolution and composition: constraints from receiver function studies. Journal of Geophysical Research 111, B02304, http://dx.doi.org/10.1029/2005JB003802.

Nguuri, T.K., Gore, J., James, D.E., Webb, S.J., Wright, C., Zengeni, T.G., Gwavava, O., Snoke, J.A., Kaapvaal Seismic Group, 2001. Crustal structure beneath southern Africa and its implications for the formation and evolution of the Kaapvaal and Zimbabwe Cratons. Geophysical Research Letters 28 (13), 2501–2504.

Paige, C.C., Saunders, M.A., 1982. LSQR: an algorithm for sparse linear equations and sparse least squares. ACM Transactions on Mathematical Software 8 (1), 43–71, http://dx.doi.org/10.1145/355984.355989.

Pasyanos, M.E., Nyblade, A.A., 2007. A top to bottom lithospheric study of Africa and Arabia. Tectonophysics 444 (1–4), 27–44.

South African Committee for Stratigraphy, 1980. Stratigraphy of South Africa. Part 1 (Kent, L.E., Comp.), Lithostratigraphy of the Republic of South Africa, South West Africa/Namibia, and the Republics of Bophuthatswana, Transkei and Venda: Handbook of Geological Survey of South Africa, 8. 690 pp.

Uken, R., Watkeys, M.K., 1997. Diapirism initiated by the Bushveld Complex, South Africa. Geology 25, 723–726.

Van der Merwe, M.J., 1976. The layered sequence of the Potgietersrus limb of the Bushveld Complex. Economic Geology 71, 1337–1351.

Walraven, F., 1987. Geochronological and isotopic studies of Bushveld Complex rocks from the Fairfield borehole at Moloto, northeast of Pretoria. South African Journal of Geology 90, 352–360.

Walraven, F., 1997. Geochronology of the Rooiberg Group, Transvaal Supergroup, South Africa. Economic Geology Research Unit, University of the Witwatersrand, Johannesburg, South Africa, Information Circular, 316. 21 pp.

Walraven, F., Darracott, B.W., 1976. Quantitative interpretation of a gravity profile across the western Bushveld Complex. Transaction of the Geological Society of South Africa 79, 22–26.

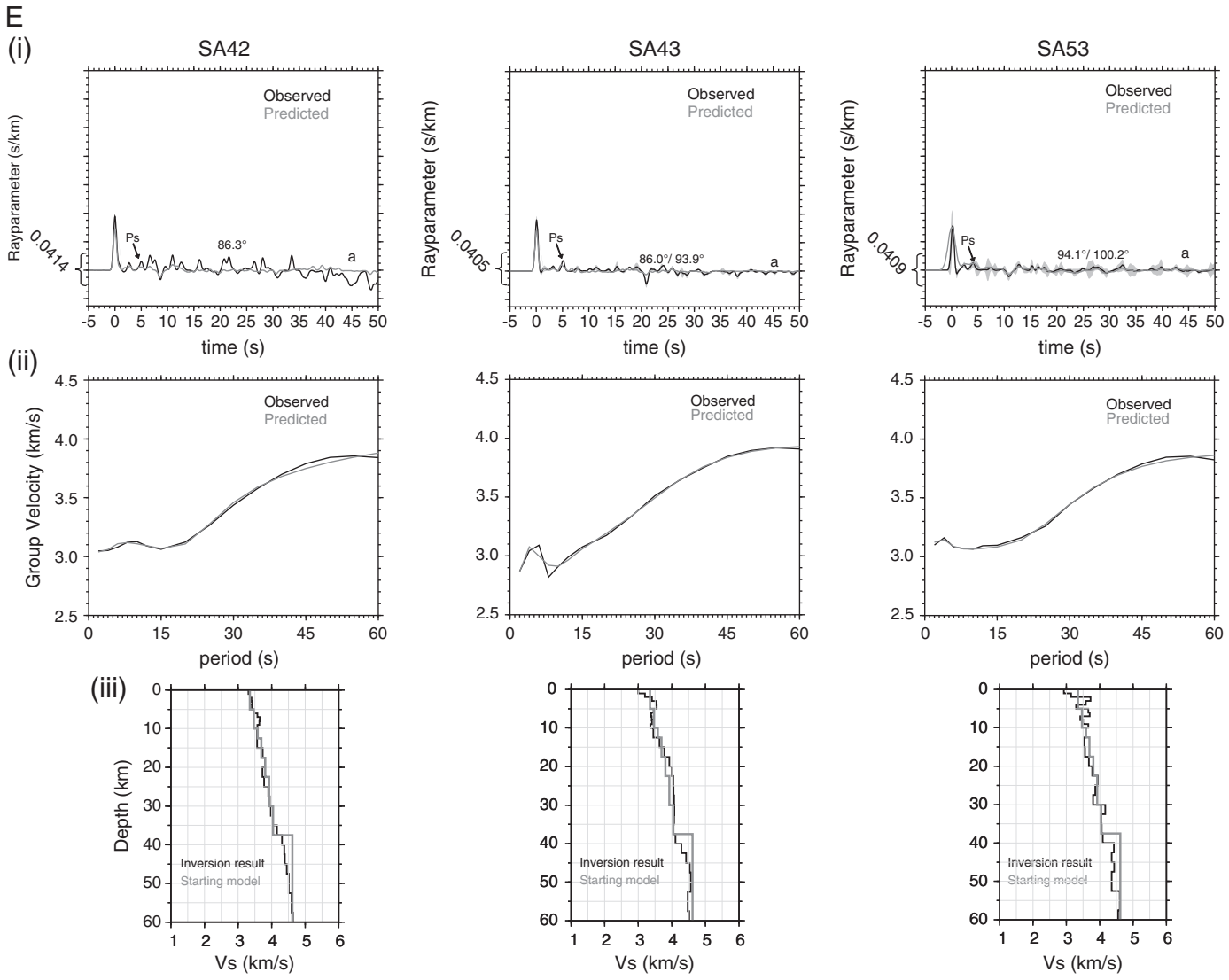

Fig. 10 (*continued*).

Webb, S.J., Cawthorn, R.G., Nguuri, T.K., James, D.E., 2004. Gravity modelling of Bushveld Complex connectivity supported by Southern African Seismic Experiment results. South African Journal of Geology 107, 207–218.

Webb, S.J., Ashwal, L.D., Cawthorn, R.G., 2010. Continuity between eastern and western Bushveld Complex, South Africa, confirmed by xenoliths from kimberlite. Contributions to Mineralogy and Petrology 162, 101–107, http://dx.doi.org/10.1007/s00410-010-0586-z.

Yang, Y., Li, A., Ritzwoller, M.H., 2008. Crustal and uppermost mantle structure in southern Africa revealed from ambient noise and teleseismic tomography. Geophysical Journal International 174, 235–248, http://dx.doi.org/10.1111/j.1365-246X.2008.03779x.

F

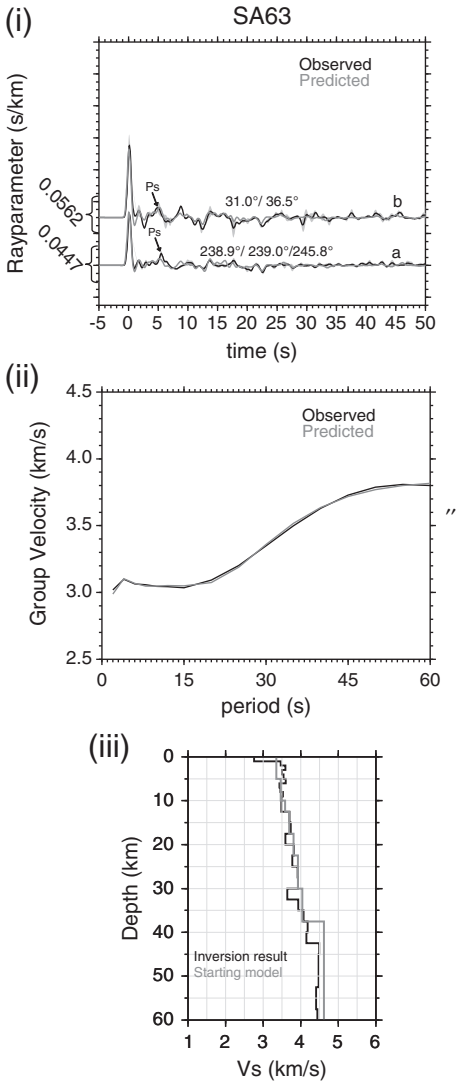

Fig. 10 (*continued*).

Table 1
Summary of crustal parameters.

Station	Back-azimuth (deg)	Vs (1–5 km depth) ± Std. deviation (km/s)	Vs (6–10 km depth) ± Std. deviation (km/s)	Vs below 30 km depth ± Std. deviation (km/s)	Crustal thickness (km)	Thickness of layers with Vs ≥ 4.0 km/s (km)	Average Vs (1–10 km depth) (km/s) ± Std. deviation (km/s)	Average Vs below 30 km depth (km/s) ± Std. deviation (km/s)	Average Crustal thickness (km)	Average Thickness of layers with Vs ≥ 4.0 km/s (km)
LBTB	46.5°	3.5 ± 0.0	3.5 ± 0.1	4.1 ± 0.0	42.5	15	3.5 ± 0.1	4.1 ± 0.1	42.5	11
	87.4°	3.5 ± 0.1	3.5 ± 0.1	4.1 ± 0.1	42.5	10				
	240.2°	3.5 ± 0.1	3.5 ± 0.1	4.0 ± 0.1	40.0	10				
	257.1°	3.5 ± 0.1	3.4 ± 0.1	4.0 ± 0.1	40.0	10				
SA39	37.4°	3.4 ± 0.1	3.5 ± 0.1	4.0 ± 0.1	40.0	5	3.5 ± 0.1	4.0 ± 0.1	40.0	5
SA40	35.0°	3.5 ± 0.0	3.6 ± 0.0	4.0 ± 0.1	45.0	15	3.6 ± 0.1	4.0 ± 0.2	42.5	12
	95.9°	3.6 ± 0.1	3.6 ± 0.1	4.0 ± 0.2	42.5	8				
SA42	86.3°	3.4 ± 0.0	3.6 ± 0.0	4.1 ± 0.1	40.0	13	3.5 ± 0.1	4.1 ± 0.1	40.0	13
SA43	90.0°	3.4 ± 0.2	3.4 ± 0.0	4.1 ± 0.1	42.5	10	3.4 ± 0.1	4.1 ± 0.1	42.5	23
SA45	35.7°	3.4 ± 0.0	3.5 ± 0.1	4.1 ± 0.1	42.5	13	3.5 ± 0.1	4.1 ± 0.0	45.0	15
	96.3°	3.4 ± 0.0	3.5 ± 0.1	4.1 ± 0.1	45.5	16				
SA46	35.0°	3.3 ± 0.1	3.6 ± 0.0	4.1 ± 0.1	42.5	10	3.5 ± 0.1	4.1 ± 0.1	42.5	10
SA47	32.5°	3.5 ± 0.2	3.6 ± 0.2	4.1 ± 0.1	45.0	13	3.6 ± 0.2	4.1 ± 0.1	45.0	11
	95.4°	3.5 ± 0.1	3.6 ± 0.2	–	–	–				
	240.0°	3.5 ± 0.0	3.6 ± 0.1	4.0 ± 0.2	42.5	8				
SA48	244.6°	3.5 ± 0.1	3.3 ± 0.1	4.2 ± 0.1	45.0	18	3.4 ± 0.1	4.2 ± 0.1	45.0	18
SA49	89.1°	3.3 ± 0.1	3.5 ± 0.1	4.1 ± 0.1	37.5	10	3.4 ± 0.1	4.1 ± 0.1	37.5	10
SA50	31.8°	3.5 ± 0.1	3.6 ± 0.1	3.9 ± 0.2	40.0	5	3.6 ± 0.1	3.9 ± 0.1	40.0	4
	157.1°	3.5 ± 0.1	3.6 ± 0.1	3.8 ± 0.1	37.5	0				
	235.9°	3.4 ± 0.1	3.6 ± 0.1	3.9 ± 0.1	40.0	3				
SA51	36.5°	3.3 ± 0.1	3.4 ± 0.1	4.0 ± 0.1	42.5	8	3.4 ± 0.1	4.0 ± 0.1	42.5	8
SA52	31.5°	3.4 ± 0.1	3.4 ± 0.0	4.0 ± 0.2	37.5	6	3.4 ± 0.1	4.0 ± 0.2	37.5	6
SA53	97.2°	3.5 ± 0.1	3.5 ± 0.3	4.1 ± 0.1	40.0	10	3.5 ± 0.1	4.1 ± 0.1	40.0	10
SA63	33.8°	3.5 ± 0.1	3.5 ± 0.1	4.0 ± 0.3	42.5	10	3.5 ± 0.1	4.0 ± 0.2	42.5	9
	241.2°	3.6 ± 0.0	3.5 ± 0.1	4.0 ± 0.1	42.5	8				
SLR	81.1°	3.5 ± 0.2	3.4 ± 0.2	3.9 ± 0.1	37.5	3	3.5 ± 0.2	3.9 ± 0.1	35.0	3
	265.3°	3.5 ± 0.2	3.4 ± 0.1	3.9 ± 0.1	35.0	3				

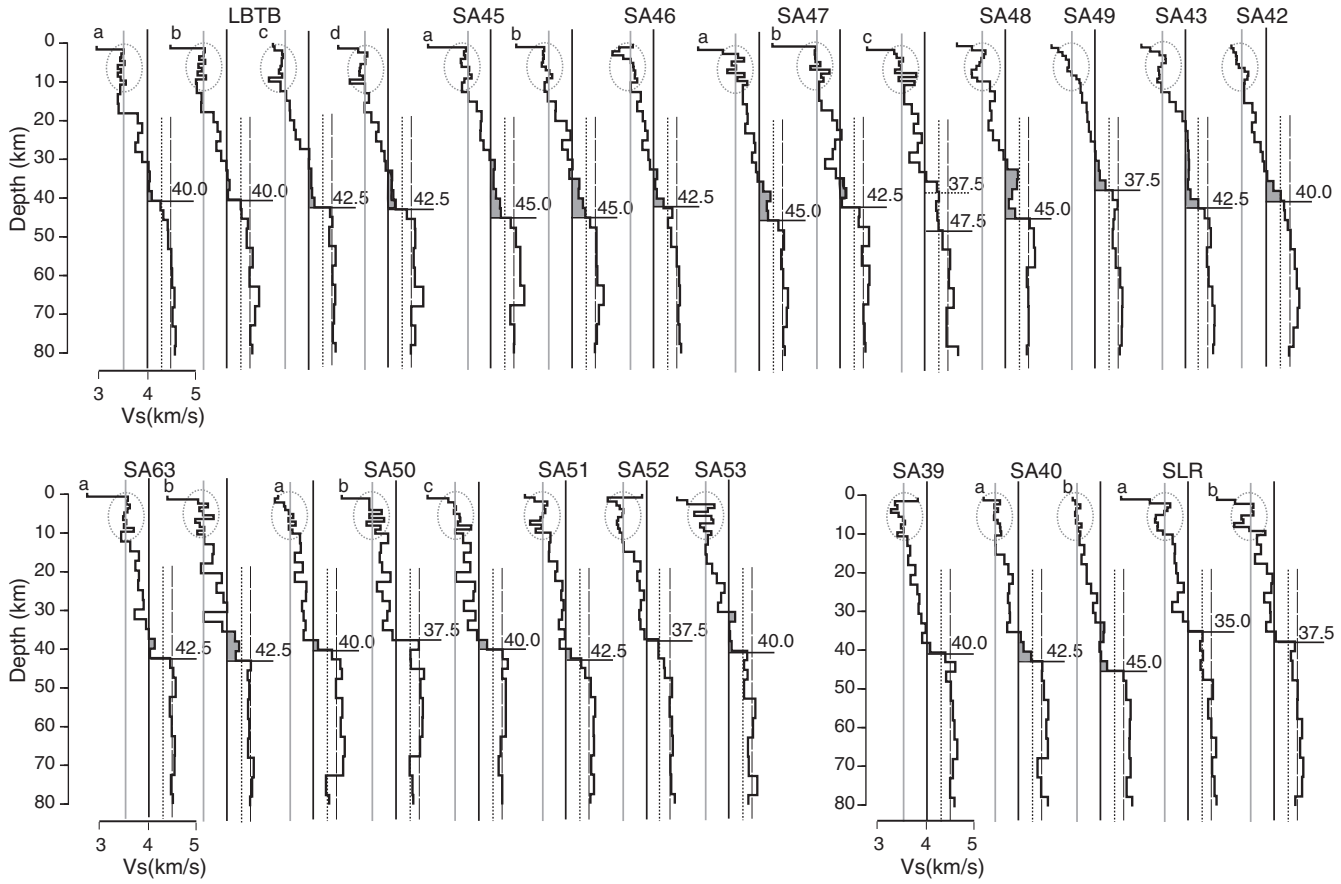

Fig. 11. A compilation of shear wave velocity profiles from joint inversion results showing Moho depths and details of the velocity structure in the upper and lower parts of the crust. The letters on top of each profile correspond to the letters on the receiver function stacks as shown in Fig. 10. The dashed ellipses enclose an area of the upper crust from 0 to 10 km depth. Crustal thicknesses are indicated with horizontal lines and numbers in km. Lower crustal layers with Vs ≥ 4.0 km/s are shaded, and reference lines at 3.5 km/s (gray solid), 4.0 km/s (black solid), 4.3 km/s (dotted) and 4.5 km/s (dashed) are shown on each profile.

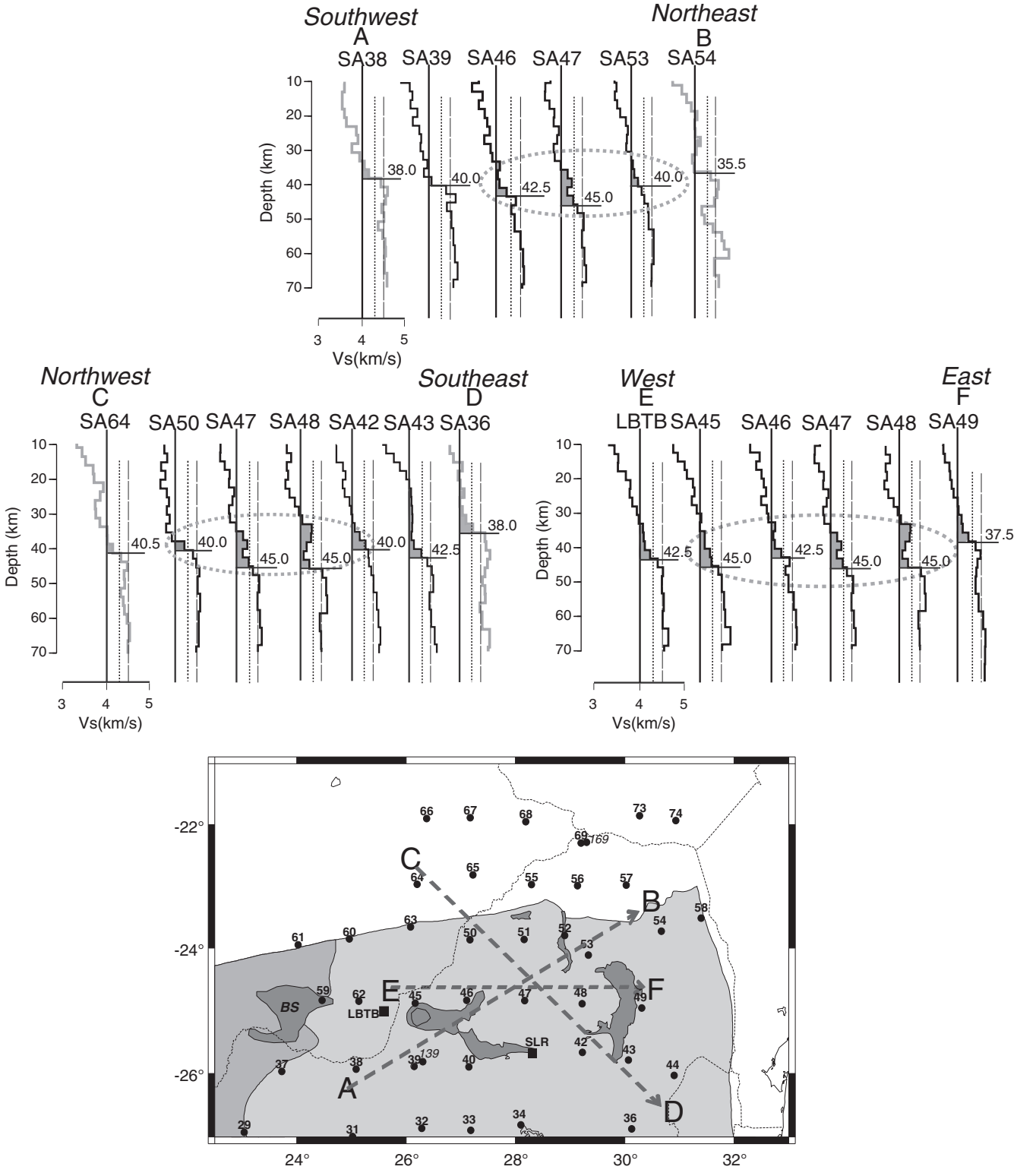

Fig. 12. Cross-section of the crust across the BC from southwest to northeast (AB), northwest to southeast (CD), and west to east (EF). The shear wave profiles in gray are from Kgaswane et al. (2009). The map shows the location of the profiles (dotted lines) and station locations. The gray shading is the same as in Fig. 2c.

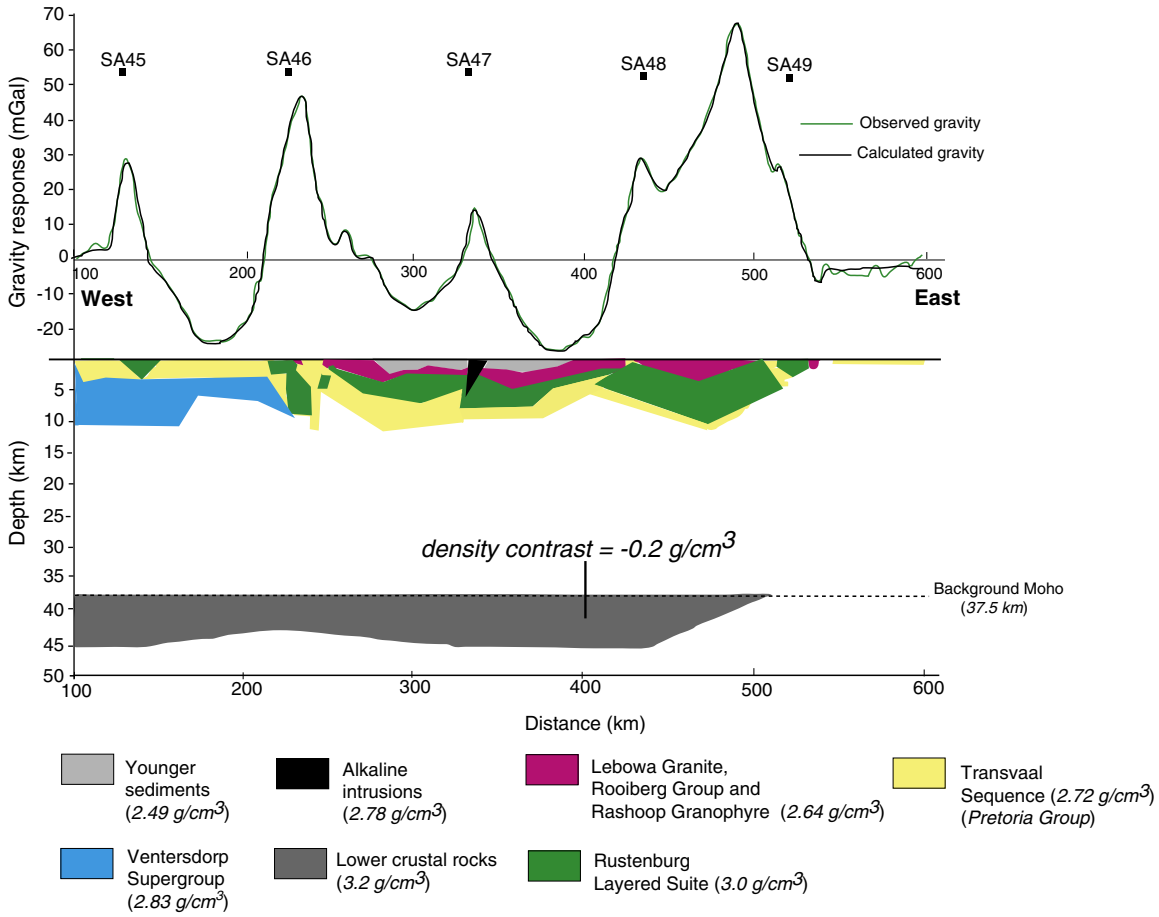

Fig. 13. Revised Webb et al. (2004) density model based on the Vs models for the five seismic stations indicated. The densities (inside brackets in the legend) for the different crustal layers are taken from Webb et al., 2004.

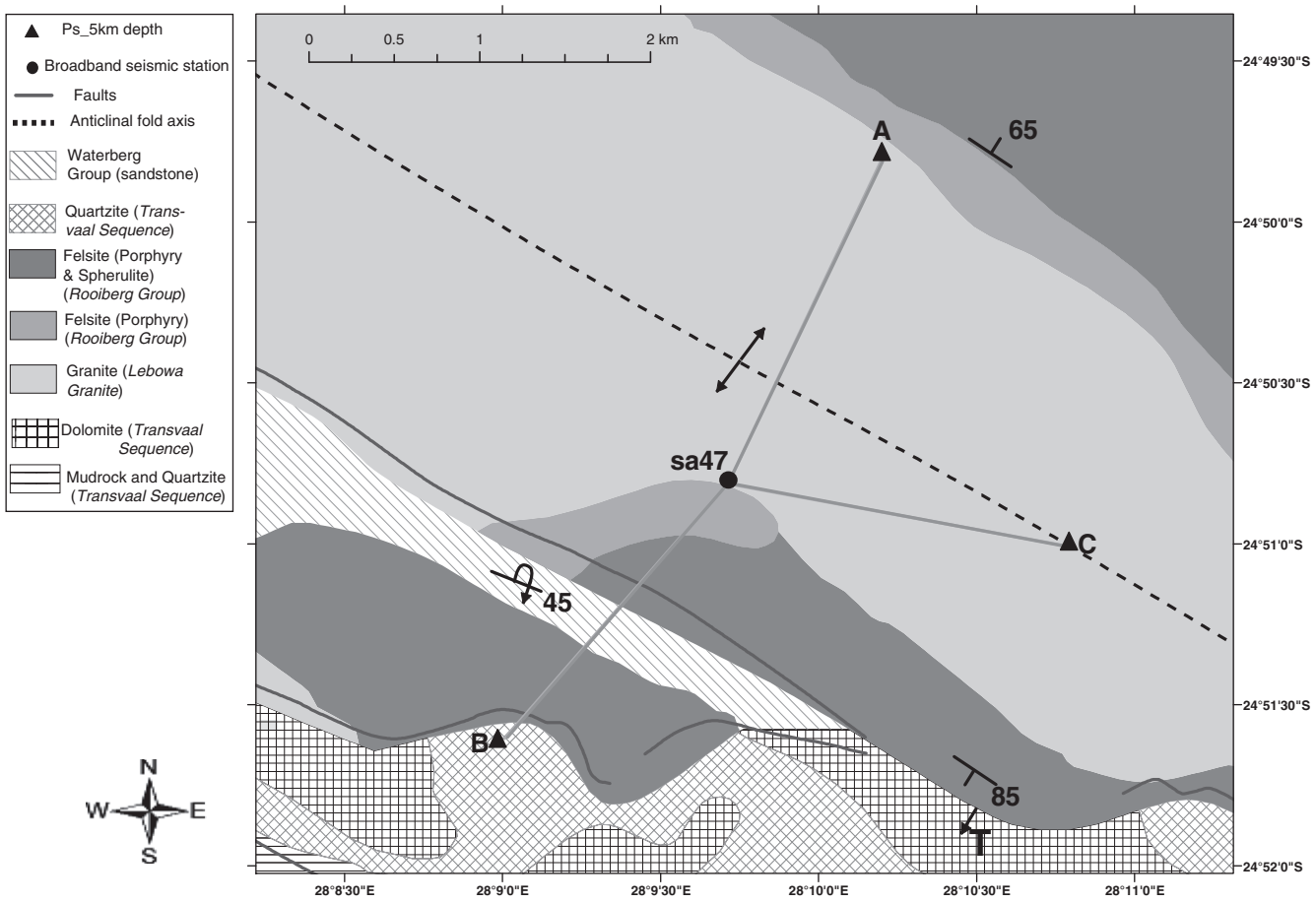

Fig. 14. Map of the local surface geology around station SA47 showing the Ps conversion points and structural relationships of the different sequences (map modified from the 1:250 000 geology map of South Africa).

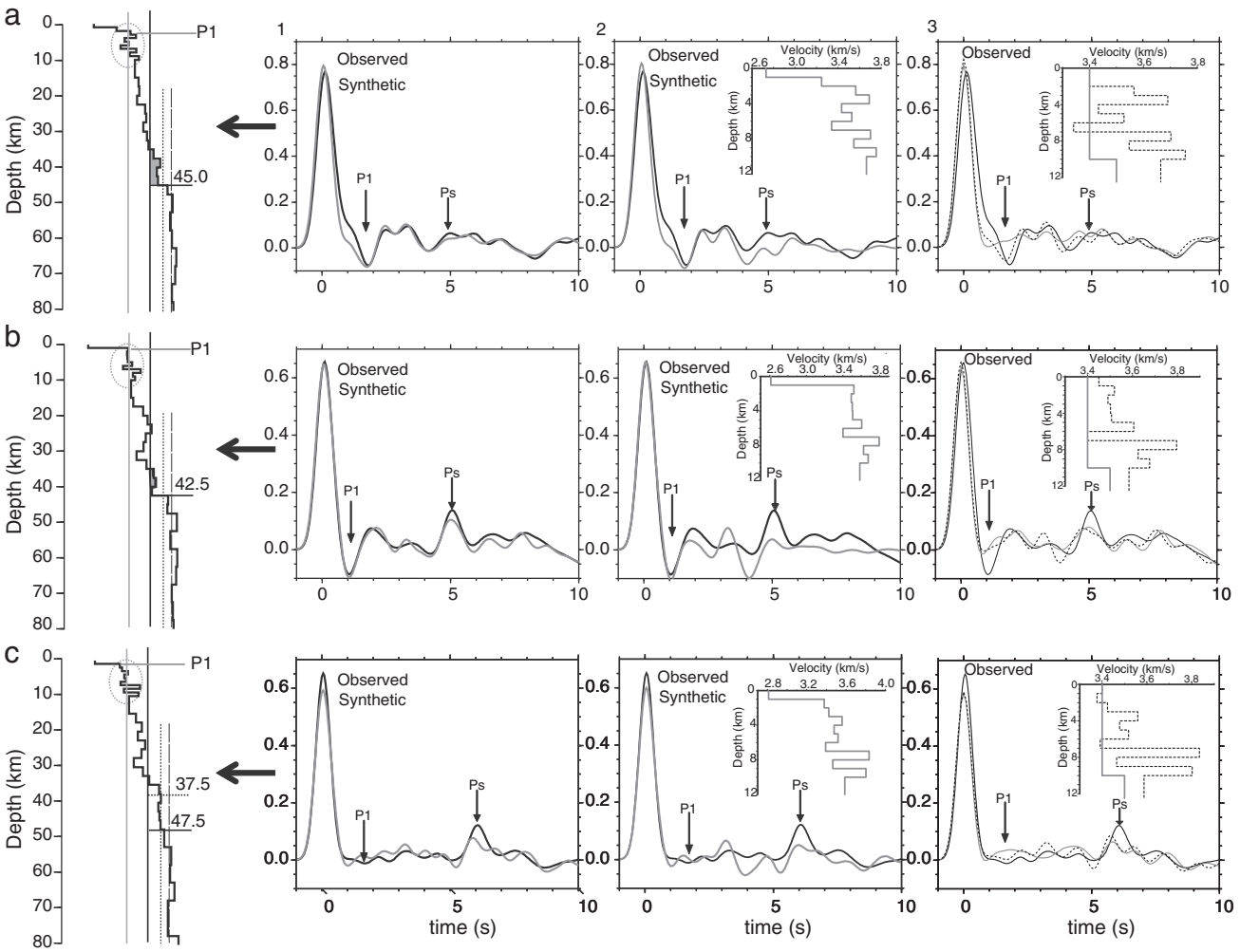

Fig. 15. Modeling results of the three receiver function stacks for station SA47 (a, b, and c). See text for an explanation of each panel.